PhD degree in Medical Nanotechnology

European School of Molecular Medicine (SEMM) and Italian Institute of Technology (IIT)

University of Milan

Faculty of Medicine

Settore disciplinare: FIS/07

AN ATOMIC FORCE MICROSCOPY BASED INVESTIGATION OF INTERFACIAL PROPERTIES OF BIOCOMPATIBLE CLUSTER ASSEMBLED THIN FILMS

Varun Vyas

University of Milan, Milan

Matricola n. R07408

Supervisor: Prof. Paolo Milani
University of Milan, Milan

Added co-Supervisor: Dr. Alessandro Podesta
Univerity of Milan, Milan

Anno accademico 2009-2010

This work is dedicated to my parents & my sister for supporting & encouraging me to pursue this degree.

“ You can know the name of a bird in all the languages of the world, but when you're finished, you'll know absolutely nothing whatever about the bird... So let's look at the bird and see what it's doing -- that's what counts. I learned very early the difference between knowing the name of something and knowing something.”

(Richard Feynman (1918 - 1988))

“Knowledge, the object of knowledge and the knower are the three factors which motivate action; the senses, the work and the doer comprise the threefold basis of action.**”**

(Bhagavad Gita)

List of Contents

List of Figures

List of Tables

Abbreviations

Ns-TiOx	Nanostrucured Titanium Oxide
SCBD	Supersonic Cluster Beam Deposition
AFM	Atomic Force Microscope
PZC	Point of Zero Charge
IEP	Isoelecric Point
NSL	Nanosphere Lithography
PMCS	Pulsed Micro Plasma Cluster Source
rms	Root Mean Square
PEG	Polyethylene Glycol
APTES	Amino propyl triethoxy silane
STM	Scanning Tunnelling Microscopy
FD	Force Distance
PSPD	Position Sensitive Photo Detector
CM	Contact Mode
FS	Force Spectroscopy
FV	Force Volume
TM	Tapping Mode
FM	Frequency Modulation
AM	Amplitude Modulation
KCl	Potassium Chloride
NaCl	Sodium Chloride

NaOH	Sodium Hydroxide
HCL	Hydrogen Chloride
Tris	Tris(hydroxymethyl)aminomethane
HEPES	4-(2-hydroxyethyl)-1-piperazineethanesulfonic acid
PBS	Phosphate Buffered Saline
HBSS	Hank's Buffered Salt Solution
BSA	Bovine Serum Albumin
XPS	X-ray Photoelectron Spectroscopy
Ns-PdOx	Nanostrutured Palladium Oxide
PVD	Physical Vapour Deposition

Abstract

Cluster-assembled nanostructured Titanium Oxide (ns-TiOx) deposited by Supersonic Cluster Beam Deposition (SCBD) recently proved to be a very promising biomaterial, allowing the adhesion and proliferation of cancer and primary cells, with no need of additional coating with extra-cellular matrix proteins, and the adhesion of proteins, such as streptavidin, with no need of additional coatings of polycations. The intrinsic nanostructure of this material, with fine granularity, high porosity and specific area, coupled to the chemical reactivity of the surface is likely to be a key element in determining the biological affinity of the material with nanometer-sized biomolecules, such as proteins. However, little is known of the specific role played by each of these surface properties in the interaction of proteins with nanostructured biocompatible materials. For understanding the role of different surface properties we used atomic force microscopy (AFM) to study morpho-chemical nature of ns-TiOx biocompatible surfaces, in particular we have characterized the adhesive properties of ns-TiOx against nanoprobes carrying chemical groups similar to those involved in protein-surface adhesion processes, and we have characterized the electric charging of ns-TiOx surfaces in aqueous medium at different pH, and how this is affected by surface roughness.

AFM Force-Spectroscopy measurements have been used to characterize local adhesive properties of ns-TiOx surfaces. In order to achieve this goal we have developed a patterning strategy based on the combined use of SCBD and Nanosphere Lithography (NSL), for the production of sub-micrometer patterns of ns-TiOx on glass and other substrates. With this methodology one can have both target and reference material in

the same investigation area. Results indicated that atoms on the surface of ns-TiOx can form coordinate bond with protein molecules thereby aiding in irreversible protein adsorption at the same time retaining complete biological activity.

To further understand how protein adsorption is affected by the buffer medium and by the surface properties of the substrate, we have measured the point of zero charge (PZC) of nanostructured cluster-assembled TiOx. As each kind of protein has different isoelectric point (IEP), hence their adsorption is greatly affected by pH of the buffering medium and concentrations of ions in the solutions. To this purpose, colloidal probes were developed to measure attractive and repulsive forces of a silica micro-sphere against metal oxide surface as a function of pH. Estimated PZC values for TiOx (rutile) and ns-TiOx is 4.9 ± 0.5 & 3.0 ± 0.5, the latter being significantly smaller than PZC typically measured on crystalline surfaces.

These results can open up new avenues towards understanding adsorption characteristics of various proteins on metal oxide surfaces.

Chapter 1 - Introduction

1.1 Objectives

The main goal of this project was to investigate mechanisms of adsorption of proteins on nanostructured metal oxide surfaces using Scanning Probe Microscopy techniques (based on atomic force microscopy - AFM), and at the same time developing novel experimental methodologies to accomplish these studies. Here we have worked with biocompatible nanostructured titanium oxide surface. Amount of protein adsorbed on nanostructured surface is influenced by roughness of the thin film, at the same time there is large contribution of surface chemistry which is responsible of chemisorption of the first monolayer of protein binding onto metal oxide surface; the interplay between these two factors is not yet well understood, and deserves a considerable amount of experimental and theoretical work

Here we have tried to define the role of surface chemistry on protein adsorption at two levels: first, the bonds that can be formed between protein molecules and ns-TiOx surface in absence of any dissolved ionic species (buffering medium); second, the role of buffering medium and pH on protein adsorption, related to the morphological properties of the substrate. Bonding behaviour between proteins and ns-surfaces was defined using force-volume measurements on nanopatterned ns-TiOx thin films. Thereafter, point of zero charge of ns-TiOx surfaces was estimated using colloidal probes in force-spectroscopy experiments at four different pH values, on samples with different surface morphology, included a reference crystalline rutile TiO_2 surface.

1.2 General Background

What is Nanotechnology? It is the study and manipulation of matter at a scale of 10^{-9} m. It is a multidisciplinary field which includes integration of different branches of physics, chemistry and biology. Its applications extend from the fields of medicine to electronics. Medical Nanotechnology is a branch of nanotechnology which involves engineering, as the interface between molecular biology and bioactive materials. Applications of such interfaces extend from the field of Nanomedicine in production of nanoparticles for drug delivery to development of nanobiosensor for detection of various medically relevant biomolecules.

A bioactive metal oxide surface should have certain physical properties towards protein and cell adhesion. Certain characteristics are common for both cell and protein adhesion because cells do not directly proliferate on a surface, but there is always a layer of protein molecules which mediates interaction of cell against its background. Therefore, by focusing on adhesive properties with respect to proteins of a material, one can comment on biocompatibility and its related issues. Protein adhesion is affected by surface roughness, which determines overall surface area available for protein adsorption, by surface charge, which is affected by surface chemistry and pH of surrounding medium, and by surface wettability describes hydrophilicity/hydrophobicity the surface.

In the present work I would like to highlight contribution of surface chemistry in protein adsorption. Main focus of the current project was to understand interfacial properties between of metal-oxide based biomaterials having strong application towards microarray technology and a novel substrate for culturing various medically relevant cell lines [4-5].

It is easier to explain protein adsorption when seen from more mechanistic point of view. Relative degree of the following contributions affects protein adsorption on any surface : (1) the intrinsic protein/material force mediated by solvent , (2) the thermodynamic stability of protein/material adhesion interface and (3) diffusion force of protein molecules. The latter two mainly depend on chemical interaction between material and protein. In the case of a protein on a surface, molecular interactions should be of non-covalent nature, like ionic, hydrophobic, co-ordinate, Van derWaals or very low degree of hydrogen bonding. In order to infer mechanisms involved in protein adsorption on a metal oxide surface, it is important to identify which intermolecular forces are involved. Such intermolecular investigations can be carried out using atomic force microscopy. It has been widely demonstrated how functionalized tips can be used for single molecule investigations [6].

The adhesion force F_{ad} is a combination of the electrostatic force F_{el}, the van derWaals force F_{vdW}, the meniscus or capillary force F_{cap} and forces due to chemical bonds or acid–base interactions F_{chem} [7]

$$F_{ad} \approx F_{el} + F_{vdW} + F_{cap} + F_{chem} \quad \textbf{(1)}$$

In aqueous medium all forces except capillary force play an import role in protein adhesion. Electrostatic force in aqueous medium is a double-layer force which arises because of surface charges at the interface. This electrostatic force between like particles is a long-range repulsive force which at low salt concentration keeps colloidal particle suspended in solution. With increasing salt concentration, especially by addition of di- and trivalent ions, the repulsive double layer force is screened, and at a critical concentration attractive short-

range van derWaals force overcome electrostatic barrier leading precipitation of colloidal solution.

Explanation of this kind of behavior is provided by DLVO theory[8-9], which quantitatively explains the role of electrostatic double layer force and van derWaals forces in adhesion between two colloidal particles in a solution[7]. At distances larger than a characteristic screening length, the Debye length (see below), this electrostatic double-layer force decays roughly exponentially. The decay length is the so-called Debye length[7]. Debye length is a measure of screening effects of ions dissolved in aqueous medium. Debye screening length ($\boldsymbol{\lambda_D}$) is inversely proportional to the square root of concentration of ions in the solution, weighted by the square of their valence:

$$\boldsymbol{\lambda_D} = \sqrt{\frac{\boldsymbol{\varepsilon \epsilon_0 \kappa_B T}}{\boldsymbol{e^2 \sum_i c_i Z_i^2}}} \qquad \textbf{(2)}$$

- **ε** & $\boldsymbol{\varepsilon_o}$ are the dielectric constant of the solution and the permittivity of vacuum, respectively
- $\boldsymbol{k_B}$ is the Boltzmann constant
- $\boldsymbol{C_i}$ is the concentrations of the ions
- $\boldsymbol{Z_i}$ is the valence of the ions
- ***T*** is the absolute temperature
- ***e*** is the elementary electric charge

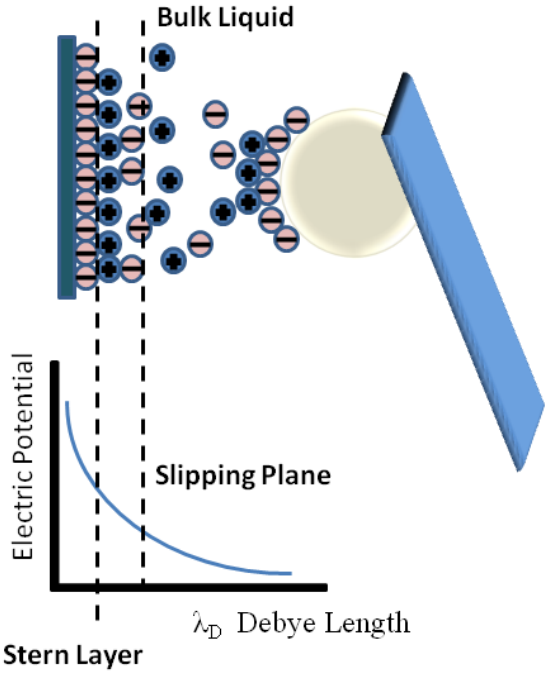

Figure 1. Schematic of electrostatic double layer effect when a colloidal probe of similar charge approaches a metal oxide surface.

The electrostatic force experienced by two surfaces in an aqueous medium is proportional to the product of their surface charge densities, these latter quantities depending on the pH of the solution. By experimentally determining electrostatic force through force-distance curves one can obtain values of surface charge densities of interacting surfaces. By comparing surface charge densities at different pH one obtains 'Point of Zero Charge' (PZC [10]) of the surface of interest, as that value of the pH at which the surface under consideration possesses a net zero electric charge. PZC is an important parameter for adsorption measurements and surface characterization. At the PZC, the surface is electrically neutral. Above or below that point, it possesses a net electric charge, and can thus interact with a protein, which, depending on its isoelectric point, will be positively or negatively charged as well. PZC influences therefore the formation of bonds between incoming protein molecules and metal oxide surfaces.

Typically, PZC value is obtained by potentiometric titrations[11] and Isoelectric point IEP value for proteins is estimated by Isoelectric focusing[12]. For potentiometric titrations large amount material is required but in our case ns-TiO_2 is produced in form of thin films. Another method for estimating PZC is by measuring electrostatic and Van Der Waals interactions with atomic force microscopy. Butt[13] and Raiteri[14] measured PZC on Mica and Silicon surfaces respectively by measuring interactions taking place between AFM probe and the target surface. In order to estimate PZC of ns-TiO_2 borosilicate colloidal probes were used. Electrostatic force experienced by the sphere of radius R (in our case colloidal probe) can be calculated by following equation:

$$\boldsymbol{f_e = \frac{2\pi\lambda_D R}{\epsilon_o \epsilon} \cdot \left[\left(\sigma_T^2 + \sigma_S^2\right) \cdot e^{-2D/\lambda_D} + 2\sigma_T\sigma_S \cdot e^{-D/\lambda_D}\right]} \qquad \textbf{(3)}$$

Where

- σ_T and σ_S are surface charge densities of AFM tip and sample surface,
- D is the distance between the tip and sample surface.
- λ_D is the Debye length as described above.

From colloidal probe experiments, both the Debye length and the surface charge densities can be obtained, by fitting the force-distance curve using Eq. 2 (or Eq. 12, see later). Charge densities, or their product, can be plotted against pH, and the pH at which charge density is zero is identified as the PZC of the surface[14]. In order to accomplish above described goals we have developed new protocols where we have coupled nanosphere lithography (NSL) with Supersonic Cluster Beam Deposition (SCBD) to produce 2D hexagonal

array of ns-TiOx and have tried to adapt this technique in other areas of materials sciences like investigating mobility of nanocluster as function of temperature. As our main goal was to define bioactive properties of titanium oxide we have developed protocols for estimating PZC value of ns-TiOx surface to understand adsorption behavior of proteins as function of pH and functionalizing AFM tips with amino acids and protein to perform force spectroscopy experiments. With force spectroscopy some groups have analyzed adhesion characteristics of protein depending upon the surface wettabilty properties and binding affinity of different functional groups that are present on the surface of the protein can be easily determined (see appendix) [6, 15]. For highlighting biocompatibility of ns-TiOx both prokaryotic and eukaryotic cell lines were grown on ns-TiOx and we have tried to describe their cell spreading function and interaction with substrate though AFM Imaging (see appendix).

For biocompatible metal oxides surfaces (in our case Cluster Assembled Titanium Oxide) it is very important to predict distribution of surfaces charges at different pH. When pH of the solution is above PZC, surface would be negatively charged and if IEP of the protein is below this pH then protein will also have net negative charge. Both protein and metal oxide surface having similar net charge, therefore lesser number of protein molecules will adsorb on metal oxide surface. Most proteins are very well characterized and their IEP can be easily found by literature survey. Therefore, by understanding surface charging behavior at different pH it might be possible to deduce interaction of proteins with nanostructured-Titanium oxide (ns-TiOx). This same concept can be extended towards other metal oxide surfaces and this also provides us with an opportunity to develop surfaces with high degree of biocompatibility.

1.3 Nanostructured Materials

Nanostructured Materials are those materials whose structural elements are made up of clusters, crystallites or molecules having dimensions in 1 to 100 nm range[16-17]. Ns-TiO_2 thin films used in this study are made of TiO_2 nanoclusters. In general synthesis of clusters and nanoparticles can be divided in to three groups[16-17] :-

- **Gas-phase cluster synthesis** – Clusters are formed in the gas phase prior to their deposition on a solid surface.
- **Self-assembled clusters on surfaces** – Clusters form on a suitable substrate according to Stranski-Krastanov(SK) and Vollmer-Weber(VW) growth modes. SK growth occurs in a layer-by-layer (i.e. 2D) fashion upto a certain thickness (which is generally related to lattice mismatch between the adsorbate and substrate) and then switches to a 3D, islanding growth mode. VW growth occurs when the adsorbate and substrate surface (and interface) free energies are such that it is thermodynamically favorable for the overlayer to form islands from the very onset of growth.
- **Colloidal synthesis** - It involves controlled nucleation and growth of clusters in a precursor-containing solution.

Synthesis of Ns-TiO_2 thin films comes under the category of gas phase cluster synthesis. Thin films are produced by Supersonic Cluster Beam Deposition (SCBD). This technique involves a Pulsed Microplasma Cluster Source (PMCS) where a He or Ar pulse is directed against a target and is ionized by a pulsed discharge fired between the target (cathode) and an electrode (anode). Plasma obtained by target ablation is passed through aerodynamic lens

system for size selection of clusters and focused beam of particles is deposited on the substrate[18-19].

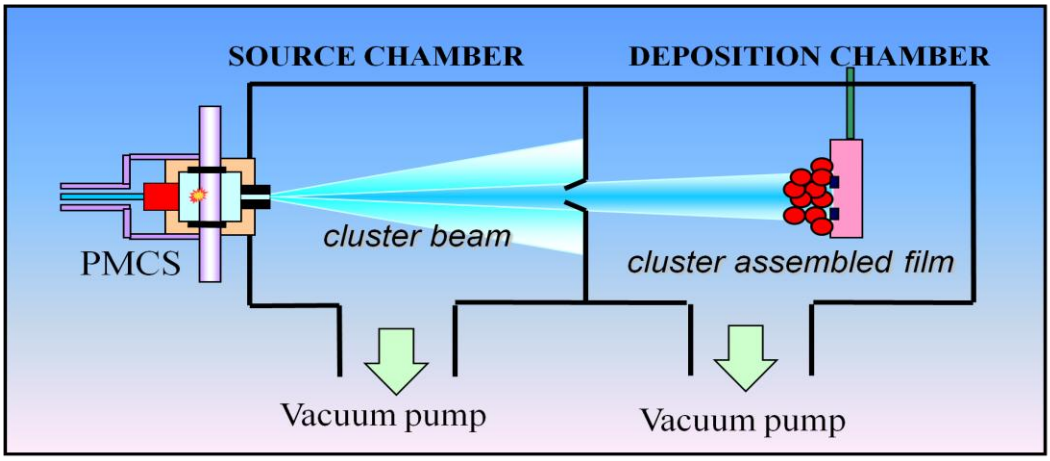

Figure 2 . Schematic of Supersonic Cluster Beam Apparatus

Figure 2 illustrates the basic design behind SCBD apparatus. Ns-metal oxide thin films of varying thickness can be easily produced by controlling the deposition time. Roughness of the sample is proportional to the thickness of the sample. Ns-TiO_2 thin films with high roughness tend to absorb more protein on their surface because of its unique nanoscale morphology[20]. Nanoscale surface morphology is described by several parameters; root-mean-squared (*rms)* roughness is one of them. *RMS* roughness of an ns-thin film is measured from AFM images. AFM topographic maps consist in N_i *x* N_j arrays of $N = N_i N_j$ heights values h_{ij} (*i,j* are the row,column indicies). The rms roughness is calculated as

$$\boldsymbol{\sigma = \frac{1}{N} \sum_{i,j} (h_{ij} - \bar{h})^2} \qquad \textbf{(4)}$$

Where $\bar{h}$ is the average height:

$$\bar{\boldsymbol{h}} = \frac{\mathbf{1}}{\boldsymbol{N}} \sum_{\boldsymbol{i,j}} \boldsymbol{h_{ij}} \qquad \textbf{(5)}$$

RMS roughness is a measure of surface corrugation, i.e. of the dispersion of surface height values around the average height $\bar{h}$. Another parameter which is taken into account for describing surface properties is *Specific Area (**S**).* Specific area is defined as the ratio of the three-dimensional area of the surface and the projected two-dimensional area. It is unity for a smooth plane, and typically larger than 1 for rough surfaces. Specific area represents the maximum accessible area to a protein or any other incoming molecule on a surface. Specific area is calculated from digitized AFM maps as:

$$\boldsymbol{S} = \frac{\mathbf{1}}{\boldsymbol{N}} \sum_{\boldsymbol{ij}} \sqrt{\mathbf{1} + \left|\boldsymbol{\nabla h_{ij}}\right|^{\mathbf{2}}} \qquad \textbf{(6)}$$

Where $\left|\boldsymbol{\nabla h_{ij}}\right|$ is the modulus of the surface gradient.

1.4 Titanium and Its Applications in Biology

Titanium is the ninth most abundant element and the second most abundant transition element (after iron) of the earth's crust. It is the first member of the 3d transition series and has four valence electrons, $3d^2 4s^2$. The most stable and most common oxidation state is IV. It is also known to show other lower oxidation states, -I,0, II, III, but it gets readily oxidized in air to Ti^{IV}. The most important oxide of titanium is the dioxide, TiO_2. Natural TiO_2 has three crystalline forms: rutile, anatase and brookite of which rutile is the most common one. Titanium oxide in its *rutile* form was discovered by German chemist M. H. Klaproth in 1795. In this work we have used rutile TiO_2 for comparative study along with nanostructured TiO_2. Titanium is known to form large number of coordination complexes. This ability of titanium to form coordination complexes with more than one type of atom can play an important role towards its application in biological sciences [2].

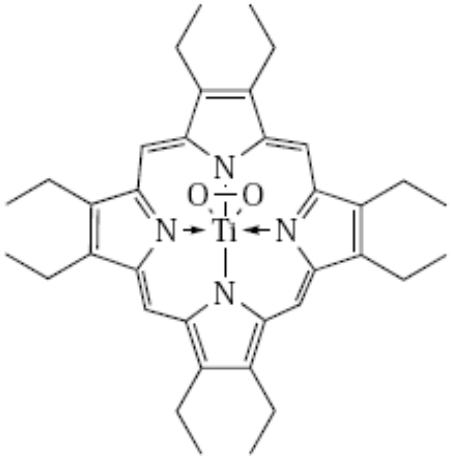

Figure 3. Octaethyl Porphyrin Derivative[2]

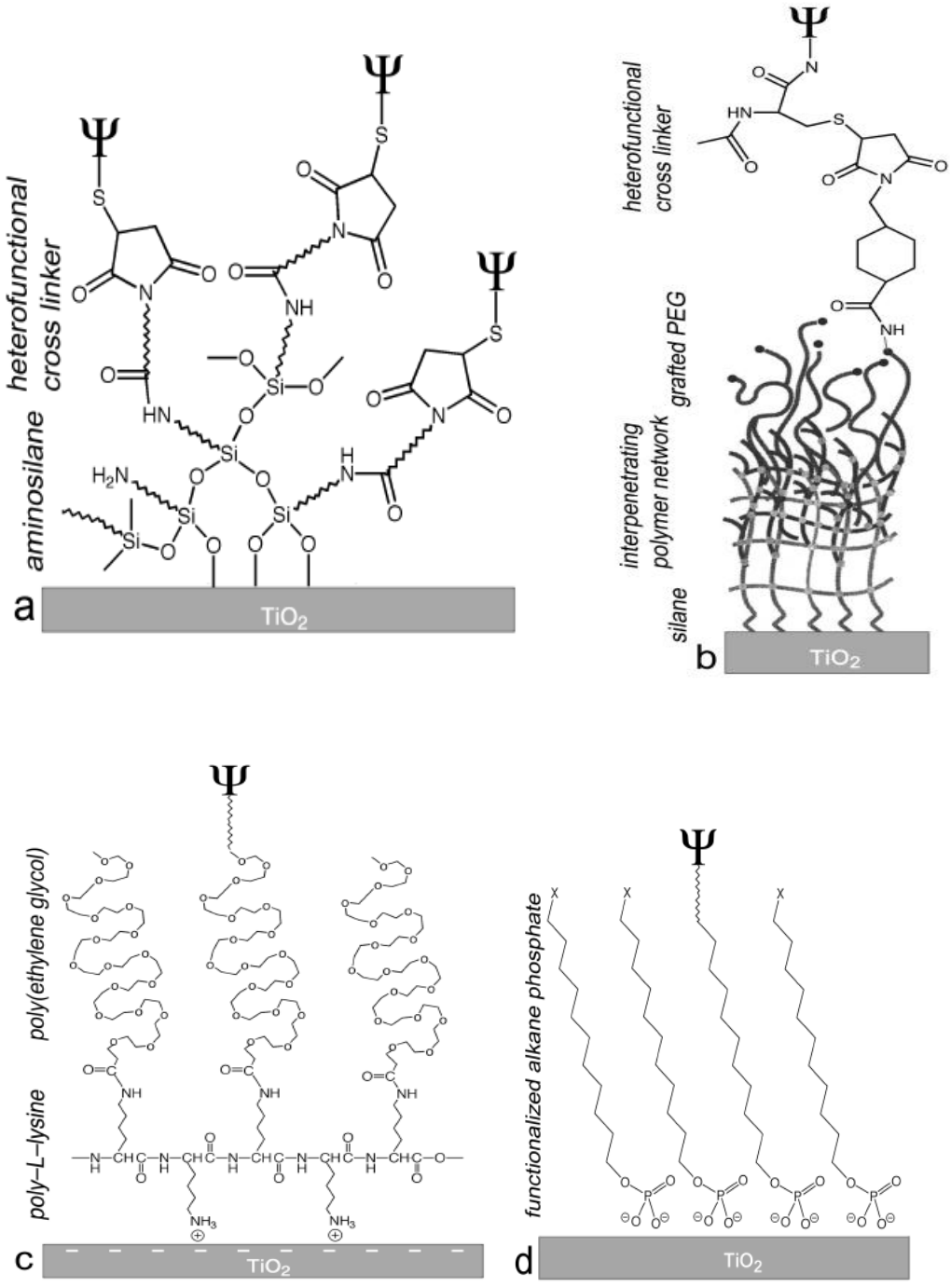

Figure 4. Different functionalization concepts for producing biomimetis surface. (a) Silanization with APTES followed by a specific peptide (Ψ). (b) silinization followed by formation of interpenetrating polymer network . Then specific peptide (Ψ) is attached via PEG and acrylamide based hetrofunctional crosslinkers. (c) polycationic poly(amino acid) with PEG is used as a base for attaching specific peptide (Ψ). (d) self assembled monolayers of long chain alkanephosphates were partially finctionalized at the terminal end with peptide (Ψ). The phosphate interacts with Ti(IV) cations through coordination complex.[3]

Titanium oxide surfaces due to their excellent inertness and biocompatibility are used in a variety of biomedical situations. To study cell and tissue specific cell response, titanium based surfaces can be easily modified by physical adsorption (through van der Waals, hydrophobic or electrostatic forces) or chemical binding of functional groups. Depending upon the application biomimetic surfaces can be produced by functionalizing TiO_2 with (3-aminopropyl)triethoxysilane (APTES), silanes, modified polyethylene glycol (PEG), etc [3]. Oxotitanium compounds can form polymeric chain like structures (-Ti-O-Ti-O-) and they can further coordinate with water molecules. Nanostructured-TiO_2 produced by SCBD contains similar chain like structure on its surface, along with under-coordinated oxygen and titanium atoms which can play an important role in stabilizing protein molecules on its surface [21]. Biocompatible nature of ns-TiOx was first demonstrated by Carbone *et al* in 2006 [5]. That work demonstrated that morphology of ns-titanium thin films mimicks that of extracellular matrix, due to film nanoscale granularity and porosity. These thin films were successfully developed as living-cell microarrays. Such microarrays are powerful tools in the field of functional genomics and drug discovery [4], allowing high throughput screening of cell phenotypes and intermolecular interactions. Adsorption mechanism of proteins like streptavidin was investigated by force spectroscopy and by valence-band photoemission spectroscopy. Results indicated that exposed carboxylic groups on protein molecules can form coordinate bond with titanium atoms on the nanostructured surface [21]. Thereafter, SCBD technique was combined with a simple micropatterning technique to generate complementary micropatterns of hydrophobic bovine serum albumin (cell-repellent) and hydrophilic ns-TiOx (cell adhesive). This demonstrated that PC12 cell could selectively grow on biocompatible ns-TiOx thin films [22]. Further more on close investigation on role of

nanoscale morphology, one could observe how proteins get trap between nanoclusters, leading to formation of layers of proteins which in turn could reciprocate basement membrane in biological systems. This basement membrane like formations facilitates growth of various cell lines [20]. The main advantage of these cluster assembled thin films is that by controlling roughness of the substrate one can modulate amount of protein that can be adsorbed on the substrate.

1.5 Atomic Force Microscopy & Related Techniques

The Atomic Force Microscope (AFM, hereafter used also as acronym of Atomic Force Microscopy technique) is an important tool for imaging surface topography at high resolution and can also be used for measuring intermolecular forces through force-distance (FD) curves. It was the invention of Scanning Tunnelling Microscopy (STM) by Binnig and Rohrer in 1982 which eventually led to the development of AFM. The main advantage of AFM over STM was imaging of non-conducting samples, which was not possible with STM. When AFM came into existence in 1986 it also opened doorway for characterization of biomolecules. Not only it became possible to study biomolecules and surfaces at single molecule level but also investigate their properties in aqueous and non-aqueous environment.

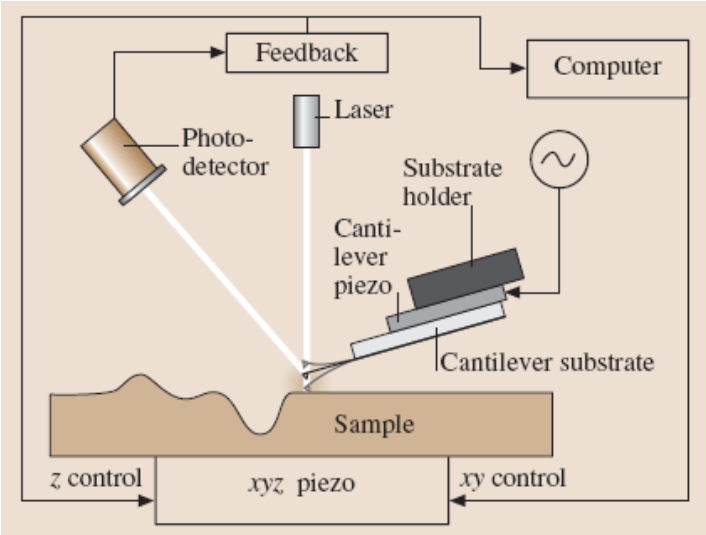

Figure 5. Working of Atomic Force Microscopy.[1]

AFMs commonly uses optical techniques to detect deflections of the cantilever. Typically, a light beam from a laser diode bounces off the back of the cantilever and it is reflected onto a position-sensitive photo-detector (PSPD) (Figure-5) [1]. This detector is divided into four quadrants in order to detect and measure both vertical and lateral displacements of the cantilever end, where the tip is located.

In general AFM imaging can be divided into two modes i.e. Static & Dynamic. They can be further divided into following sub-categories [1, 23]:

1. **Static Mode –** In this mode the static deflection of the cantilever is used as an input for the feedback to track topography; alternatively, it is converted into a force and used to map tip/surface interactions.
    a. **Contact Mode (CM)** - In contact mode the tip apex is in direct contact with the sample's surface, and the forces between the atoms of the tip and the sample are counter balanced by the elastic force produced by the deflected cantilever. Forces between the tip and the surface are attractive van der Waal forces, and capillary forces (which are always present in air and originate in a thin water surface) [24], electrostatic forces. Cantilevers used in contact mode have a very low spring constant (typically between 0.1-5 N/m), providing high sensitivity to weak forces and avoiding undesirable influence of the tip on the sample [1]. During scanning, the feedback system maintains a constant value of the cantilever deflection, and consequently, of the interaction force. A drawback of contact mode is the direct mechanical interaction of the tip with the sample. It frequently results in the tip breakage and/or sample surface

damages and it causes dragging forces associated with the lateral movement of the tip in contact with the sample[25]. Contact technique is therefore not appropriate for analysis of soft samples (organic materials or biological objects).

b. **Force Spectroscopy (FS)** - This method typically produces a force vs. distance curve, which plots the force (deflection) experienced by an AFM cantilever (via the tip) in Z direction as a function of tip-sample separation in Z. Force-distance curves were first used to measure the vertical force that AFM tip applies to the surface in contact AFM imaging. A typical force distance curve is shown in Figure 6 [5].

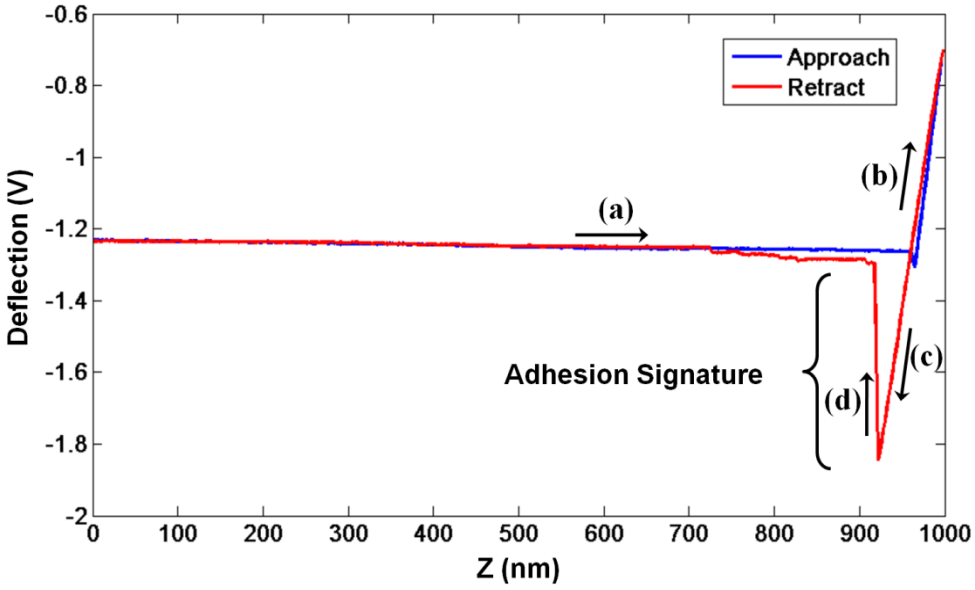

Figure 6. A Typical Force vs. Distance Curve.

During approach to the surface (a), when the tip gets very close (few nanometers) to the surface, attractive forces cause a sudden cantilever bending towards the surface. The jump of the tip in contact to the surface is due to the large gradient of the attractive forces near the sample surface (Figure 6 - Jump-In). The jump of the tip to the surface is observed when the cantilever elastic constant is smaller than the force gradient. During the further approach of the probe to the sample, the tip starts experiencing a repulsive force, and the cantilever bends in the opposite direction (Figure 6 - point b). The slope of the curve in this region is determined by the elastic properties of both sample and cantilever. During the forward motion the shape of curve is strongly influenced by the capillarity and plasticity effects. The capillarity effect is due to the liquid layer often present on the sample surface in an ambient environment (typically, this layer is mostly water). In figure 6 (point c) the hysteresis due to capillarity effect is clearly visible. As the probe approaches the surface, the tip is wetted by the liquid (at jump-in distance) and a water meniscus is formed. The tip therefore is affected by an additional attractive force due to capillary adhesion, and upon contact is established, by additional adhesion force due to van der Waals interaction. During retraction (c), separation occurs at larger distance (pull-off distance), required to overcome adhesion forces. A sudden jump (d) is then observed in the force curve, the depth of this jump corresponding to the adhesion force. Thus by understanding the shape of the force-distance curve it is possible to obtain quantitative information about the tip-surface interaction: not only adhesion, but also surface elasticity from the analysis of the contact (loading) portion of the curve (b).

Force of adhesion **(F_{ad})** is obtained, according to Hook law:

$$\boldsymbol{F = -k \cdot \delta x} \qquad \textbf{(7)}$$

multiplying the cantilever vertical deflection $\boldsymbol{\delta x = Zsens \times CD}$ by the cantilever force constant (***k***). The cantilever deflection is obtained multiplying the output of the photodetector (**CD**) by the deflection-sensitivity (**Zsens**), which is the inverse slope of the contact region of the curve (where it is assumed that neither the tip nor the surface are deformed upon loading). The force of adhesion, in units of nano-newtons, can therefore be obtained from the measured deflection (in Volts), using the calibration constants k and Z-sens:

$$\boldsymbol{F_{ad} = k\left(\frac{nN}{nm}\right) \cdot Zsens\left(\frac{nm}{v}\right) \cdot CD(v)} \qquad \textbf{(8)}$$

c. **Force Volume (FV)** - Force volume imaging is a method for studying correlations between tip-sample forces and surface features by collecting a data set containing both topographic data and force-distance curve laterally resolved in x-y direction. Each force curve is collected as described above except that the sample is also translated in x-y plane between two consecutive force-curves. The comparison between the topography image and the force volume images at various heights can give information about the lateral distribution of different surface and/or material properties [26-27]. A typical example of force volume

experiment can be seen in figure 7. This experiment was conducted on hexagonal pattern of ns-TiOx produced by nanosphere lithography coupled with SCBD.

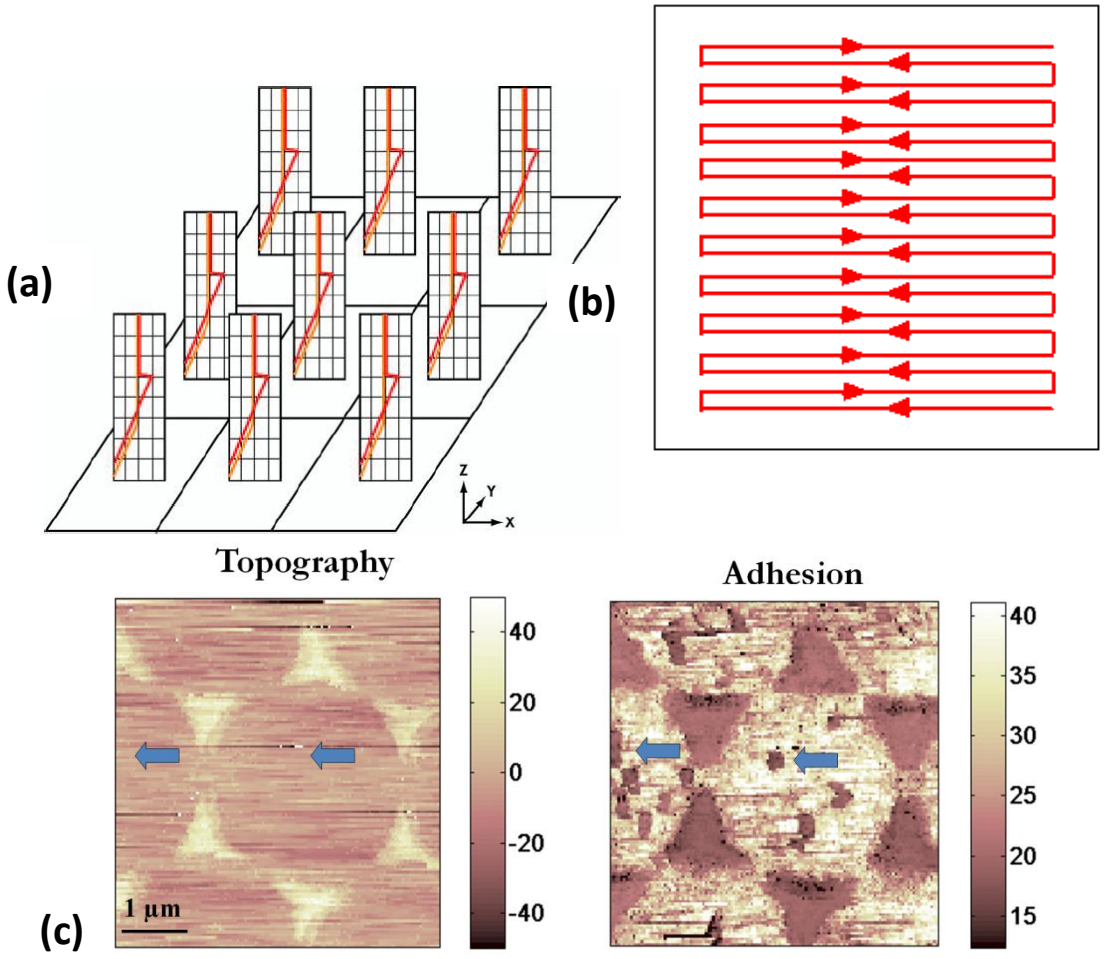

Figure 7. (a-b) Schematic description of a Force Volume experiment. A number of deflection (force) vs. distance curves like the one shown in (a) are acquired along a grid that spans a finite area on the surface, as schematically shown in (b). Upon acquisition of each single force curve, the AFM software calculates the local relative height of the surface, and uses these values to build the topographic map (c -left). Force curves are then post-processed using custom Matlab routines and adhesion force values are extracted as the difference between the average non-interaction value and the bottom of the adhesion well. The resulting adhesion map (c -right) is in one-to-one correspondence with the topographic map. The adhesion map of a ns-TiOx pattern reveals small features that are not visible in the topography (which is often noisy in liquid), highlighting nanoscale heterogeneities in surface chemistry, and possibly in surface morphology.

2. **Dynamic Mode** - In this mode cantilever is deliberately vibrated. There are two basic methods of dynamic operation: amplitube modulation (AM) and frequency modulation (FM) [28].

   a. **Tapping Mode (TM) or Amplitude Modulation (AM)** - Tapping mode is most commonly used AFM mode. This technique maps topography by lightly tapping the surface with an oscillating probe tip. The cantilever oscillates at a frequency near its resonance frequency and the oscillation amplitude is monitored. In this way the interaction of the tip with the sample is drastically reduced with respect to CM and therefore this technique is appropriate for the analysis of soft samples and for the analysis of very weakly immobilized soft-objects as biological objects [29]. In TM, feedback system compares the amplitude of cantilever oscillations (in CM the cantilever deflection) to the setpoint. The amplitude of cantilever oscillation is in order of a few tens of nanometers and the frequency of resonance of a cantilever is of hundreds of KHz (in air or in other gasses).

   b. **Non-Contact Mode or Frequency Modulation (FM)** – This mode was developed to achieve true atomic resolution with AFM in UHV. The cantilever is oscillated at a fixed amplitude at its resonance frequency.This resonance frequency depends on force acting between tip and the sample surface. In FM-AFM, the spatial dependence of the frequncy shift induced in the cantilever motion by the tip sample interaction is used as the source of the contrast. Thus, the topography in the images represents a map of constant frequncy shift over the surface.

Chapter 2 - Probing Nanoscale Interactions on Biocompatible Cluster Assembled Titanium Oxide Surface.

To characterize local adhesive properties of ns-TiOx surfaces along with a control surface, a patterning strategy was developed to have both target and reference material in the same investigation area. Sub-micrometer patterns of ns-TiOx were produced on amorphous silicon oxide (glass) surface by coupling SCBD with NSL. These nanopatterned nanostructured surfaces were investigated for morpho-chemical properties through AFM based force spectroscopy measurements.

Interaction between silicon nitride tip and nanostructured surface should be similar to the interactions between protein and ns-TiOx. Therefore, force spectroscopy measurements on nanopatterned ns-TiOx substrate can help us to have better understanding of intermolecular interactions at protein-TiOx interface.

2.1. Materials & Methods

2.1.1. Supersonic Cluster Beam Deposition

Nanostructured titanium oxide thin films are deposited over amorphous borosilicate coverslips (Ted pella) with a diameter of 13 mm. Coverslips are first cleaned in ethanol twice, by sonication for 10 mins. Thereafter, they are placed in a mask for deposition. The deposition is carried out by rastering a beam of clusters produced with a Pulsed Cluster Plasma Source across a substrate in a Supersonic cluster Beam Apparatus (SCBD). Rastering produces a uniform coating of nanostructured thin film on the substrate. Depending upon the application, one may produce samples with different thickness and roughness. After each deposition, samples are annealed at 250^{O} C for 2 hrs for removal adsorbed atmospheric contaminants, and are stored in vacuum.

2.1.2. Nanosphere Lithography

Any kind of experimental work requires verification which is done by conducting a control experiment. In the case of investigation of ns-TiOx properties, the control consisted in measuring the same interactions on a well known, reference surface: a smooth silica coverslip (amorphous silicon oxide). ns-TiOx and silica are both oxide, but they differ in roughness and surface chemistry. In order to have both analyte and control sample on a single substrate, on a scale accessible to AFM, we have coupled SCBD with Nanopshere Lithography (NSL), in order to produce patterned ns-TiOx films on amorphous silica. The same technique has been used to produce nanostructured TiOx patterns onto a crystalline, smooth, rutile TiO_2 substrate (see Chapter 4). NSL is very

widely used technique which has application in producing plasmonic nanostructures, as well as highly ordered arrays of carbon nanotubes, etc [30-31].

Here we have first spin-coated 3 micron polystyrene beads on glass coverslip. A monolayer of polystyrene beads with hexagonal symmetry is then obtained, and serves as a contact mask for the deposition of a film of ns-TiOx by SCBD. After the deposition sample is sonicated to remove mask of beads: The resulting pattern can be investigated by AFM in tapping mode in order to characterize surface morphology.

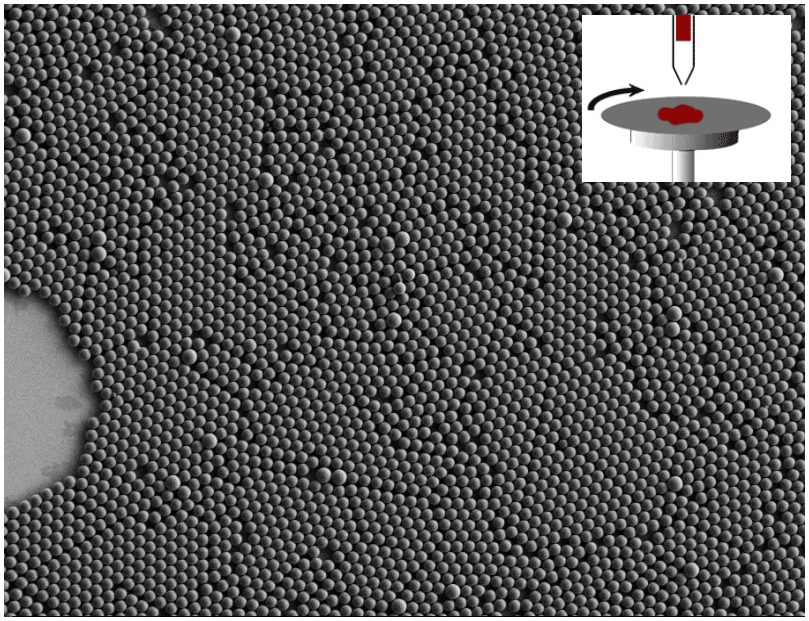

Figure 8. SEM Image of monolayer of polystyrene beads (Size-3 micron) produced by spin coating (Top Right)

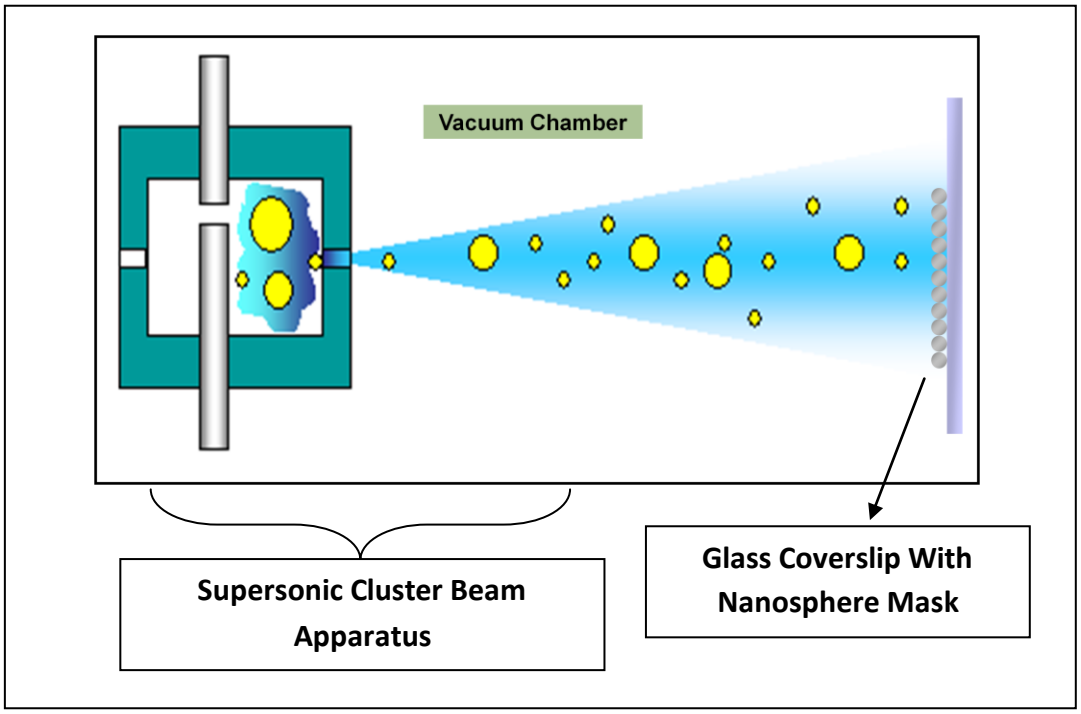

Figure 9. Deposition of Nanoclusters in Supersonic Cluster Beam Apparatus Over a Nanosphere Mask of Polystyrene Beads.

Before NSL all glass coverslips are cleaned using piranha solution (a mixture of H_2O_2 and H_2SO_4 30% acid solutions, in ratio 1:3) for 10 minutes. This step removes adsorbed organic contaminants plus also makes surface more hydrophilic by addition of hydroxyl groups on the surface. This increased wettability of the surface facilitates spread of latex (polystyrene) spheres during spin coating. 3 µm latex spheres were bought from Duke Scientific and original concentrate is diluted twice with a 1:400 Triton-x/Methanol solution. After removal of the spheres by sonication a 2D hexagonal array is produced. With this 2D array one can simultaneous investigate two surfaces in one single experiment. This decreases the possibility of any unknown ambiguities which may arise if the two surfaces are examined in separate experiments.

Besides surface chemistry other parameters like surface mobility, crystallization varying temperature, etc. can be studied. With this method concurrent investigation of scattered nano-clusters and thin films can be easily carried out (See Appendix).

2.1.3 Force Volume Imaging.

After the removal of the spheres, sample is imaged by AFM in tapping mode in order to visualize nanoscale patterns. This is followed by Force-Volume (FV) imaging (Veeco) of the as-deposited and annealed samples, both in air and in milli-q water, in order to obtain maps of nanoscale adhesion correlated to topography. Milli-Q water refers to ultrapure laboratory grade water that has been filtered and purified by reverse osmosis. It's free of any dissolved ions which may passivate the TiOx surface during longer measurements. Force spectroscopy involves taking force-distance (FD) curves over every point corresponding to a pixel of the AFM image. FD curves were acquired on a 3 x 3 μm^2 micron sized area containing two triangular islands of ns-TiOx along with reference glass substrate. Resolution was kept to 128 curves for each scanned line, acquired at 4 Hz scan rate, with a resolution of less than 1 nm per pixel.

Data obtained from FV maps was analyzed using Matlab routines; forces measured on ns-TiOx and glass surface are segregated in order to calculate average values of adhesion force. Gold coated Contact Si_3N_4 cantilevers (DNP-20) were purchased from Digital Instruments-Veeco Metrology (Santa Barbara, CA). These silicon nitride tips were used without any chemical modifications. Spring constant of cantilevers used were determined using thermal noise method [32]. Before start of each experiment, Z-sens is calculated on hard substrate like glass coverslip both in air and water.

2.2 . Results

2.2.1. Morphology of uniform and patterned ns-TiO_x films

The typical morphology of ns-TiO_x patterns produced on the amorphous silica surfaces is shown in Figure 10. In the main box the regular hexagonal arrangement of triangular ns-TiO_x islands can be seen. While the area covered by the pattern was estimated by optical microscopy to be about 1 mm^2, typical extension of ordered regions is below 100 μm. Defects related to the primeval sphere mask are clearly visible, in the form of missing ns-TiO_x islands, or areas uniformly coated by ns-TiO_x, corresponding to extended regions where spheres were absent. The inset in the bottom-right corner of Figure 10 shows a high-resolution AFM image acquired in the region marked by the arrow, showing the peculiar nanostructured morphology of ns-TiO_x films. The granular, high specific-area, nanoporous structure of ns-TiO_x film is a consequence of the low-energy deposition regime typical of SCBD [19] , and of the ballistic deposition regime, where size-dispersed clusters impinge on the surface and stick without significantly diffuse [33]. The size of the smallest units observed in the inset is at the nanometer level, larger units result from the coalescence of single TiO_x clusters, which already takes place in the cluster beam. We have shown that the morphological properties (roughness, specific area) of thin ns-TiO_x films can be tuned reliably acting on the deposition time, i.e. on the film thickness [34]. The films used in this study had typically thickness of 30 nm, and rms roughness of 5-10 nm. We also acquired high-resolution images of the ns-TiO_x patterned domains, in order to characterize their geometry and verify that during the lithographic process the nanostructure of the film is preserved. One such

image is shown in the inset in the top-left corner of Figure 10. Each nearly-triangular island in the 2D lattice of ns-TiO_x had a linear dimension of 900 ± 100 nm. Ns-TiO_x islands were nearly flat, the tilt of their side-walls being below 5°. The average separation between adjacent islands was approximately 700 nm.

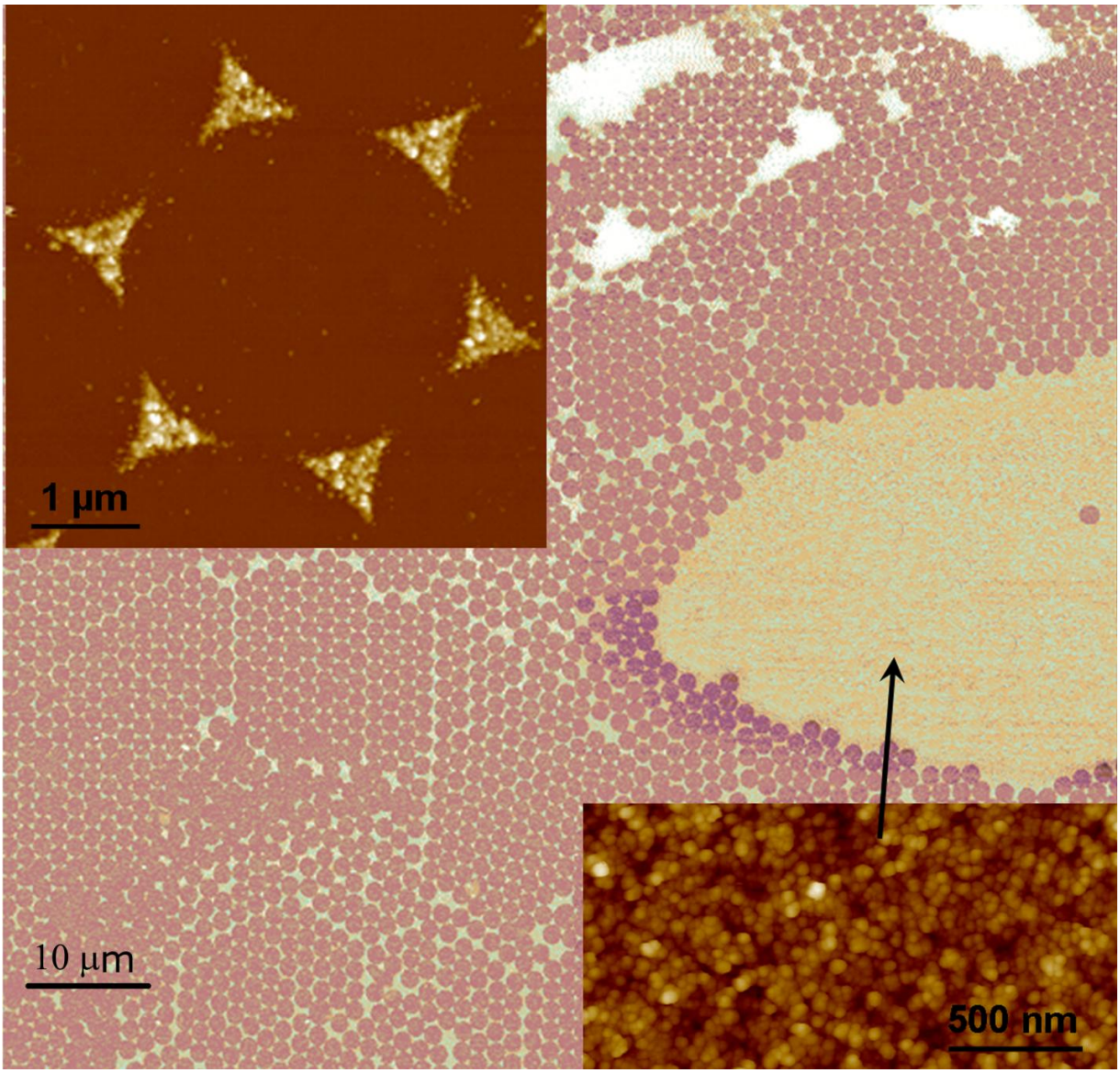

Figure 10. A wide area (100 x 100 µm^2) image of a ns-TiO_x patterned film deposited on a glass cover-slip substrate. This image has been obtained merging four 60 x 60 µm^2 AFM topographies. Ordered regions with hexagonal symmetry of nearly-triangular ns-TiO_x islands are separated by local and extended defects, reflecting the defects in the primeval sphere mask. In the top-left inset, a high magnification image of an ordered region is shown. The typical nanostructure of ns-TiO_x films can be appreciated in correspondence of extended defects (indicated by the arrow) where a uniform film is present (bottom-right inset). Vertical range of the image (black to white) is 50 nm.

2.2.2 Mapping nanoscale adhesion properties

In Figure 11 we show representative adhesion maps recorded on as-deposited and annealed samples, in air and in water (corresponding topographies are not shown; see Figure 7 (c) for an example of a topography-adhesion map pair). The close correspondence between topography and adhesion maps allowed segregating adhesion events on glass and on ns-TiO_x, such that average values for both interfaces could be calculated and compared. In order to get rid of uncertainties due to possible changes in the AFM tip radius, the ratios of average adhesion values on ns-TiO_x and glass were evaluated and used for comparison instead of the absolute adhesion values. These ratios are reported in Table 1. Nanoscale details are visible in the adhesion maps (see also Figure 7 (c)), demonstrating the high spatial resolution of this technique. It is clear from Figure 11 that there was contrast reversal in adhesion when moving from air to Milli-Q water. In humid air (40 % relative humidity), adhesion was higher on glass than on ns-TiO_x; in MilliQ water, the opposite is true. We will present and discuss the results of FV experiments in air and in MilliQ water separately, because the interpretation of data requires different interaction models.

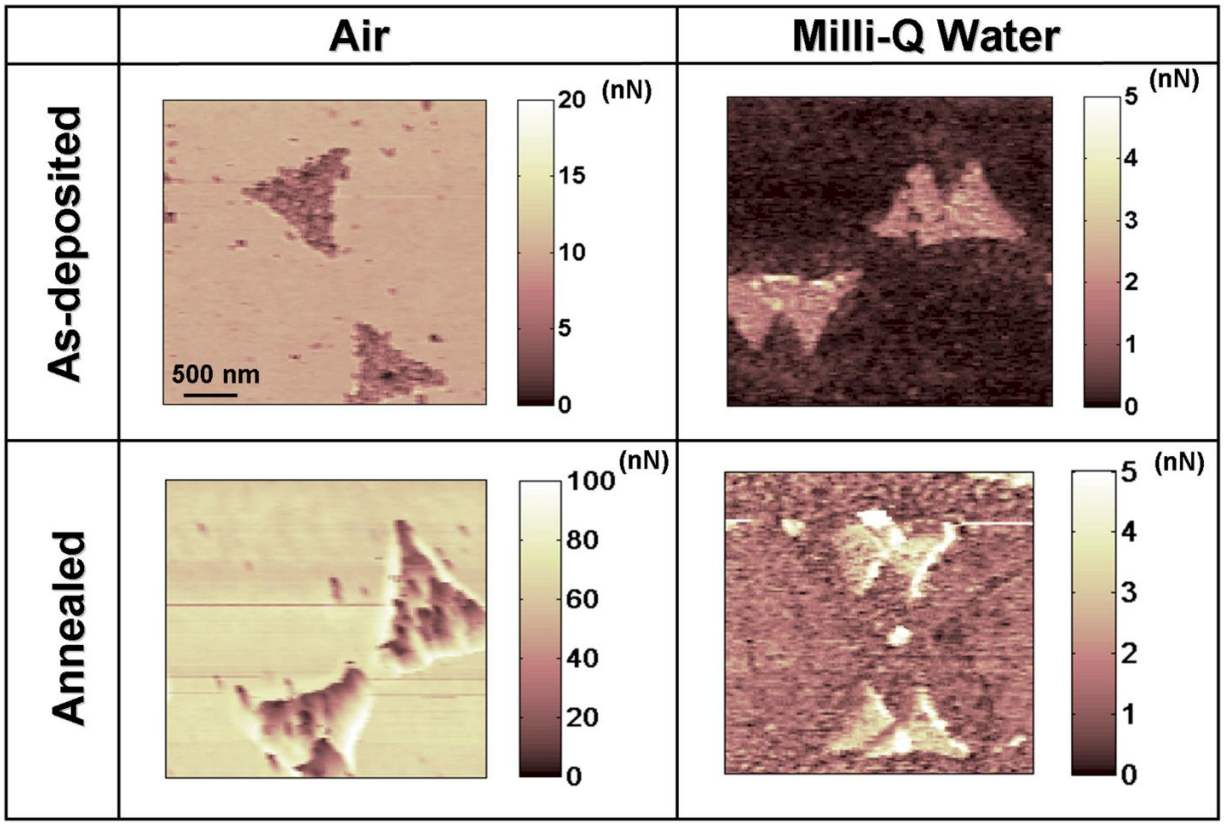

Figure 11. Representative adhesion maps measured on annealed and as-deposited samples, in humid air and in MilliQ water (pH 5-6). Doubled features observed in some maps are not due to double-tip effects; they are due to the displacement of microspheres in the mask during the deposition of ns-TiOx, probably induced by mechanical vibrations during the rastering of the sample holder, or by changes in the water menisci at the spheres' basements upon insertion in the high-vacuum chamber. A strong argument in favor of this interpretation is that there are smaller isolated features with heights comparable to those of the islands that are not doubled at all (not shown).

	Sample treatment	Adhesion ratio ($A_{ns\text{-}TiOx}$ / A_{Glass})
Air	As-deposited	0.90 ± 0.03
	Annealed	0.89 ± 0.03
Water	As-deposited	3.8 ± 1.7
	Annealed	3.5 ± 1.9

Table 1. Ratios of adhesion forces measured by AFM on ns-TiO_x and glass cover-slip surfaces.

2.3. Discussion

2.3.1 Adhesion in air

According to the data shown in Table 1, in humid air the amorphous silica surface was more adhesive towards the AFM tip than the ns-TiO_x surface. This can be understood by considering that in these conditions adhesion is dominated by capillary forces, originating from the water meniscus that bridges the two surfaces [24].

The capillary force F_{cap} between a plate and a sphere is:

$$\boldsymbol{F_{cap} = 2\pi R\gamma[\cos(\theta_1) + \cos(\theta_2)]} \quad \textbf{(9)}$$

Here R is the tip radius, γ is the surface tension of the liquid, θ_1 and θ_2 are the contact angles of the liquid on the two surfaces (Figure 12).

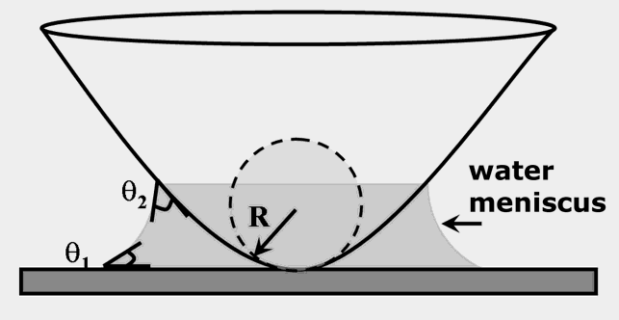

Figure 12. Schematics of the water meniscus bridging the AFM tip and the sample surface when they are at close distance or in contact in humid air environment. R is the radius of curvature of the tip, θ_1 and θ_2 are the contact angles of the liquid/surface and liquid/tip interfaces, accordingly.

Although the contact geometry in our case was not exactly that of a sphere on a flat, and although the above equation is valid only in the case of a quasi-static tip-surface

separation (i.e. at equilibrium, otherwise the constant meniscus volume model should be used, see Ref. [24]), we can take it as a good base for a qualitative discussion of our experimental data. Through the term $\cos(\theta_1)$, the surface energies of the glass and ns-TiO_x surfaces enter the equation. $\cos(\theta_1)$ is a measure of the wettability of the surface, being typically below 30° on hydrophilic surfaces, and above 60°-90° on hydrophobic surfaces. The contact angle θ_1 of a liquid on a flat homogeneous surface like that of the glass cover-slips is related to surface energies by Young equation:

$$\boldsymbol{\cos(\theta_1) = (\gamma_{SV} - \gamma_{SL})/\ \gamma_{LV}} \qquad \textbf{(10)}$$

where γ_{LV}, γ_{SV} and γ_{SL} are the surface energies at the liquid/vapor, solid/vapor and solid/liquid interfaces, respectively.

The contact angle θ_1 on a rough surface, like ns-TiO_x, can be better described by the Wenzel equation [35]:

$$\boldsymbol{\cos(\theta_1) = r\cos(\theta_0)} \qquad \textbf{(11)}$$

where r is the specific area ($r > 1$ on a rough surface), and θ_0 is the contact angle of the chemically homogeneous, atomically smooth surface.

A recent study of the wettability of ns-TiO_x thin films showed that as-deposited ns-TiO_x surfaces are mildly hydrophobic ($\theta_1 \approx 90°$), and hydrophobicity increases remarkably with increasing roughness and specific area, following a Wenzel-like behavior, up to a nearly super-hydrophobic regime ($\theta_1 \approx 140°$, and $\cos(\theta_1)$ negative and close to -1) [34]. Piranha-

treated glass is in turn very hydrophilic (cos (θ_1) positive and close to 1). Substituting these values of cos(θ_1) in Equation (8) for glass and ns-TiO_x one finds that adhesion is stronger on glass, in agreement with the experimental observations. A rough morphology on a hydrophobic material surface can hamper the meniscus formation, thereby reducing the force of adhesion. Adhesion ratios in air did not change after annealing; this suggests that annealing increases the wettability of the two surfaces by the same factor. The increased wettability of the two surfaces upon annealing can be explained in terms of removal of physisorbed hydrophobic organic contaminants and of the recovering of OH groups bonded to undercoordinated Ti or Si atoms [34, 36].

2.3.2 Adhesion in water

Adhesion measurements in ambient (humid) conditions are in agreement with the models relating wettability to morphological surface properties. In these conditions capillary interactions dominate the adhesive behavior of surfaces, hindering the specific interactions between functional groups on both tip and sample surface. Adhesion forces measured in water are up to a factor of 50 smaller in magnitude than those measured in humid air. In the liquid medium, weaker molecular interactions may dominate adhesion. Because the molecular interactions that are responsible of such adhesion forces are supposed to play an important role in determining the adhesion of proteins and biomolecules on surfaces, it turns out that nanoscale adhesion measurements in liquid medium can provide insights on the molecular bonds that are relevant in biological adhesion processes.

The ratios between adhesion forces measured on ns-TiO_x and glass are unbalanced in favor of ns-TiO_x: the latter is 3.5-4 times more adhesive than glass, while in air the relative

strength of adhesion of glass was only 10-15% larger than on ns-TiO_x. The observed differences between glass and ns-TiO_x in water can be understood, at least qualitatively, by examining the different contributions to the total interaction force. In aqueous solution, adhesion is typically the (overall attractive) sum of several terms: van der Waals (vdW) interaction, electrostatic interaction, and specific chemical bonding. While the first and the third terms are always attractive in our case, the second term can be either repulsive or attractive, depending on the buffer conditions.

Vdw force at the closest separation distance between medium 1 and medium 2 interacting in medium 3 (water, in our case) is proportional to the Hamaker constant A_{132} [37] , and also depends on the roughness of the two surfaces [38]. According to the Lifshitz theory, the room-temperature asymmetric Hamaker constant A_{132} can be calculated from the knowledge of the following parameters: static dielectric constants (ε_1, ε_2, ε_3,), average frequency of absorption <f> in the UV-VIS range (<f> = $(f_1+f_2+f_3)/3$), and corresponding refractive indices (n_1,n_2,n_3) (see Equation 11.13 of Ref. [39]). We have used the following values of the optical parameters: $\varepsilon_3 = 80$, $n_3 = 1.333$, $f_3 = 3\cdot10^{15}$ s^{-1}; $\varepsilon_2 = 7.4$, $n_2 = 1.988$, $f_2 = 2.3\cdot10^{15}$ s^{-1}; $\varepsilon_1 = 3.82$, $n_1 = 1.448$, $f_3 = 3.2\cdot10^{15}$ s^{-1} for SiO_2; $\varepsilon_1 = 80$, $n_1 = 1.72$, $f_1 = 0.9\cdot10^{15}$ s^{-1} for ns-TiO_x. The latter values of ε and n have been determined by rescaling the values for the crystalline bulk TiO_2 by the measured density of ns-TiO_x [40]. For the ns-TiO_x/H2O/Si_3N_4 system, we obtained $A_{132} = 3.7\cdot10^{-20}$ J, while for the SiO_2/H_2O/Si_3N_4 system we obtained $A_{132} = 1.7\cdot10^{-20}$ J. The ratio of calculated Hamaker constants is 2.2, but it likely becomes much smaller when the effect of the surface corrugation of ns-TiO_x is considered. Roughness is known indeed to reduce adhesion between rigid surfaces [38]. It turns out that vdW

interactions alone cannot account for the experimentally observed contrast reversal of adhesion between glass and ns-TiO_x.

The electrostatic contribution to adhesion was due to the effective surface charge density of the two interacting surfaces, which depends in turn on the dissociation degree of their surface groups in water. At zero separation, the pull-off force (adhesion) could be affected by the presence of a net repulsion or attraction due to surface charge. The pH of Milli-Q water used in our experiments was about 5-6. At this pH, the surface of amorphous silica is negatively charged, the isoelectric point (pH_{IEP}) of silica being 2-3. The approaching regions of the force curves acquired on Si_3N_4 and ns-TiO_x on both as-deposited and annealed samples reveal a net repulsive interaction (Figure 13); we conclude that our ns-TiO_x films and Si_3N_4 tips are both negatively charged at pH 5-6, i.e. their pH_{IEP} is below 5-6. This conclusion is consistent with published results. The pH_{IEP} of Si_3N_4 is reported to vary between 4.2 and 7.6 [41] , depending strongly on the silanol/silamine (or O/N) ratio, while the pH_{IEP} of Si_3N_4 AFM tips has been directly measured in force-spectroscopy experiments as $pH_{IEP} = 6.0 \pm 0.4$ [42], or pH_{IEP} = 4-5 [43](significant batch-to-batch as well as experiment-to-experiment variations can be expected). The pH_{IEP} of crystalline TiO_2 is reported to vary between 3.2 and 5.8, depending on crystalline orientation [44], while the pH_{IEP} of ns-TiO_x is still unknown (see Chapter 4; this work provides a first experimental determination of this parameter). What is relevant to the purpose of determining the leading interaction between Si_3N_4 and ns-TiO_x in liquid is that the electrostatic repulsion is the same for amorphous silica and ns-TiO_x, as can be seen by comparing the average approaching curves of the two materials (insets of Figure 13 (a)-(b)), which overlap; we exclude therefore that electrostatic interactions play a relevant role in determining adhesion reversal between glass and ns-TiO_x.

We then considered the contribution of specific chemical bonds to the adhesion of the Si_3N_4 AFM tip on glass and ns-TiO_x, starting with hydrogen bonds. In aqueous medium, Si_3N_4 surfaces undergo hydrolysis to produce silanol and silylamine (secondary and/or primary) surface groups [43, 45-46]. Depending on the annealing or chemical treatment, clean silica surfaces can have up to 4.6 ± 0.2 hydroxyl groups per nm^2 [47]. Tamura et al. report that the number of hydroxyl groups on metal oxides is almost the same [48] , thus we can expect the same number of hydroxyl groups on clean ns-TiO_x and glass surfaces. After deposition of ns-TiO_x, both the amorphous silica and the titanium oxide surface undergo similar passivation from environmental hydrocarbons, and later on they get similarly re-hydroxylated upon the thermal treatment. It follows that the number and types of hydrogen bonds that can form between silanol and silylamine groups of the Si_3N_4 surface and the hydroxyl and oxygen groups of both silica and ns-TiO_x are similar [49]; therefore the contribution of hydrogen bonding to adhesion is expected to be similar.

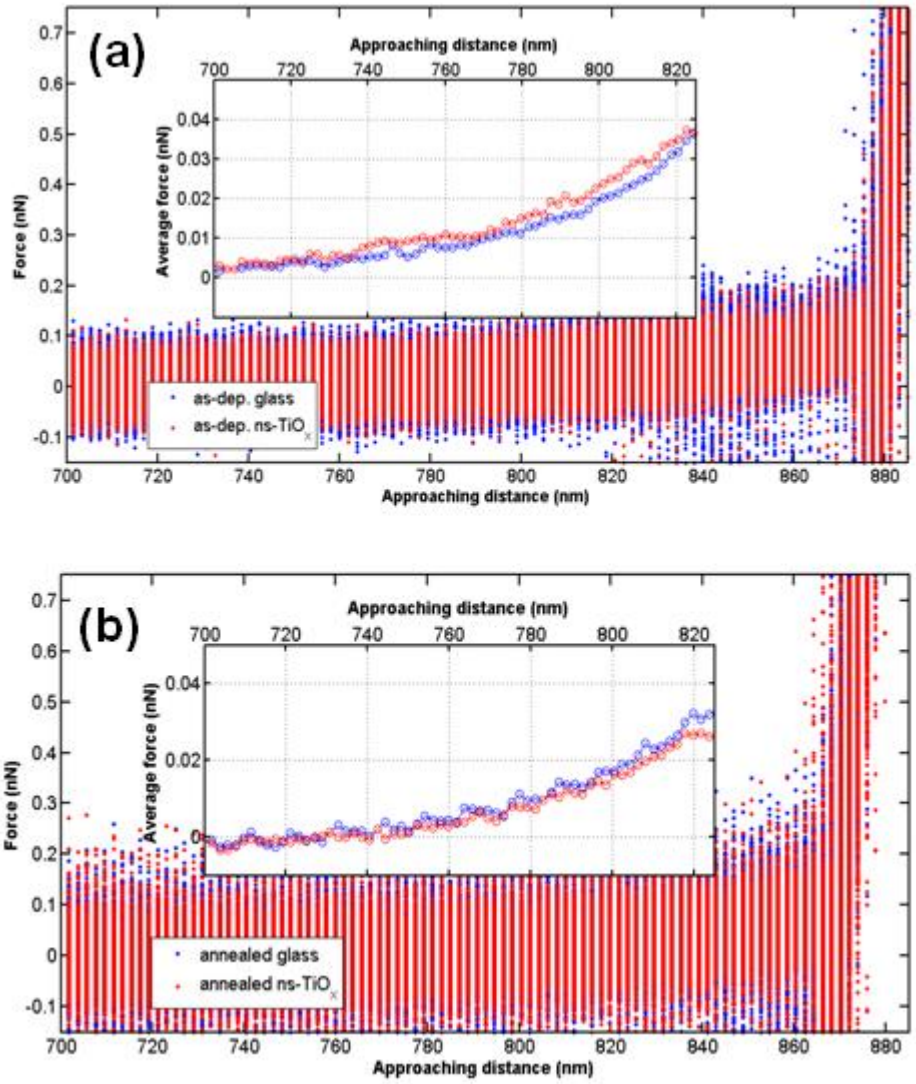

Figure 13. Approaching force-distance curves measured on (a) as-deposited, and (b) annealed ns-TiO_x patterns on glass within the same FV experiments. 128x128=16384 curves of glass and ns-TiO_x are shown together for comparison. The insets show the average approaching curves, showing a net electrostatic repulsion between the AFM Si_3N_4 tip and both glass and ns-TiO_x. Remarkably, the repulsive force has the same intensity for both materials. For the as-deposited pattern jump-into-contact takes place for both materials at a relative approaching distance of 10 nm. For the annealed sample, jump-in on ns-TiO_x is scattered between 10 and 60 nm; the latter circumstance determines the apparent deviation of the average curve from that of glass.

The factor determining the observed reversal in adhesion contrast could be ability of titanium to form co-ordinate (dative covalent) bonds with nucleophiles like oxygen or nitrogen. These bonds are stronger than hydrogen-bonds, and are peculiar of transition metal oxides; therefore they are not expected to take place on silica. Ti^{3+} and Ti^{4+} cations

form co-ordination sphere with water and hydroxyl molecules that are in equilibrium with the surrounding aqueous medium [2-3]. At the interface of the two surfaces, incoming species having lone pairs of electrons can replace chemisorbed molecules or can donate their lone pairs to under-coordinated titanium atoms thereby forming coordination bonds between the two surfaces. This concept is illustrated in Figure 14(a) where incoming silanol and silylamine groups containing oxygen and nitrogen, accordingly, can donate their extra lone pairs of electrons forming coordination complexes with titanium atoms on the nanostructured surface. Incoming nucleophiles can also displace hydroxyl groups or water molecules already bonded to Ti atoms (Figure 14(b)) and establish new co-ordinate bonds.

Previous study of the surface chemistry of ns-TiOx films by photoemission spectroscopy techniques [50-52] have shown that as-deposited ns-TiO_x films get oxidized very quickly as soon as they are exposed to air. It follows that the value of x for ns-TiO_x is very close to 2. The residual substoichiometry is due to defects (undercoordinated Ti atoms, oxygen vacancies) located on the surface of nanoparticles and at the boundaries between nanoparticles, these latter defects being typical of cluster-assembled materials. Hydroxyl groups produced by the dissociative absorption of water and chemisorbed water contribute to the healing of undercoordinated defects [53-55]**.** Annealing at moderate temperatures (typically below 250°C) further improves the oxidation of the Ti nanoparticles, favors the hydroxylation of the surface and the reorganization of defects. The scheme we present in Figure 14, with all the Ti and O atoms at their place, is therefore realistic. We can consider the surface of our ns-TiO_x films, as-deposited and annealed, as almost fully oxidized/hydroxilated, and neglect any possible influence of the oxidation state on coordinate bonding.

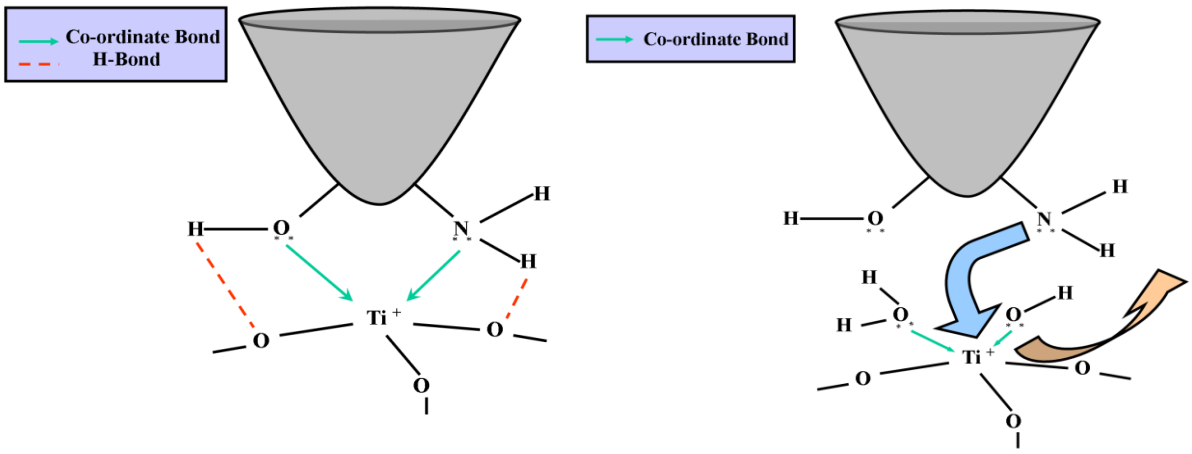

Figure 14. Schematics of the suggested chemical bonds formation between the Si_3N_4 AFM tip and the ns-TiO_x surface. (a) Incoming nitrogen and oxygen atoms can form co-ordinate dative covalent bonds with undercoordinated Ti atoms, sharing a lone pair of electrons. Concurrent hydrogen bonding can also take place, further improving adhesion; (b) Incoming nitrogen and oxygen atoms from the tip surface can also displace hydroxyl groups and water molecules already chemisorbed to the ns-TiO_x surface.

Along with the coordination complex formation, there is likely an additional contribution coming from hydrogen bonding between the ns-TiO_x surface and silanol and silylamine groups on the AFM tip, which may further increase the overall force of adhesion of AFM tip to the nanostructured surface. This concept is illustrated in the Figure 14(a). Rough morphology of nanostructured thin films may offer a higher number of sites for the formation of such coordination complexes between the two surfaces.

We were not able to observe any significant difference in water between the average adhesion values measured on annealed and as-deposited ns-TiO_x (while the contrast in the adhesion map decreased upon annealing, mostly because a marked widening of the distribution of adhesion values measured on glass); this can be related to the fact that adhesion is primarily determined by the formation of co-ordinate bonds at undercoordinated Ti sites. After annealing the percentage of available Ti sites does not change significantly,

because these sites will always be in co-ordination with adsorbed water species or other impurities that adsorb on the surface instantaneously after exposing sample to air. These Ti atoms on the annealed samples will be all available to form new co-ordinate bonds with the incoming nitrogen or oxygen atoms of the AFM tip surface, as they were in the as-deposited samples.

It is worth mentioning that the direct measurement by AFM in Force-Spectroscopy mode of breaking of co-ordinate bonds between a transition metal, Ni, and oxygen, has been recently reported [45] [56]. Here we have studied the adhesion mechanisms between a Si_3N_4 AFM nano-probe and the surface of biocompatible nanostructured TiOx. Remarkably, the chemical moieties that according to our explanatory scheme are involved in the adhesive interaction are also present in the outer surface of proteins and therefore are supposed to play a similar role in protein-surface adhesion. Surface of a protein is decorated by many oxygen and nitrogen –containing groups. They can effortlessly take part in strong co-ordinate bonding with transition-metal oxide surfaces. The concurrent formation of hydrogen bonds can produce very strong binding of proteins with ns-TiOx. This kind of interaction has been previously suggested where BSA was tested against different metal oxides, including TiOx [57]. Potentiometric proton titration on positively charged (Titania, Zirconia, etc) or negatively charged (Silica) metal oxides suggested that negatively charged groups on BSA molecules, mostly carboxyl groups, were oriented toward both the positively and negatively charged metal oxide surfaces [57-59]. The interaction of charged groups on proteins (or, in our model experiment, on the AFM tip) with metal oxide surfaces is pH-dependent, therefore the pH of the solution and the isoelectric point (IEP) or the point of zero charge (PZC) of the oxide surface may have a strong influence on the adsorption of proteins onto metal oxide

surfaces. It is therefore very crucial to correctly estimate isoelectric points of both metal oxide surfaces and proteins, because the charging behavior of both depends on them. This in turn will affect adsorption, structure, and functional activity of the proteins. Estimation of PZC of TiOx surface was the next step to develop better understand behavior of a biocompatible metal oxide surface.

Chapter 3 - Charging Behaviour of Ns-TiOx in Aqueous Buffer

Charging behavior of any surface can only be understood by measuring point of zero charge (PZC). PZC value can tell us that at certain pH value what will be charge on the surface. For measuring surface charge on TiOx substrate a borosilicate colloidal probe of known PZC can be used. Then by measuring repulsive or attractive forces against the surface of interest one can estimate PZC value of the surface. These measurements are conducted at different pH value.

These measurements were conducted in very dilute buffer to avoid any screening effect of the ions dissolved in the aqueous medium. Buffer of four different pH values (3,5,7 & 9) was prepared and a collection of FD curves were collected at each pH value on substrates having different roughness & specific area, and one crystalline substrate as a reference.

3.1 Materials & Methods

3.1.1 Production of Colloidal Probes

Rectangular tipless cantilevers with nominal force constants of 3 N/m and 0.2 N/m (NanoAndMore, Gmb) were used to produce colloidal probes for PZC estimation of ns-TiOx surface, according to the procedure described in details in Ref. [61]. Borosilicate glass microspheres with nominal radius of 5 μm were purchased from SPI (SPI supplies, West Chester, PA 19380, USA).

Standard rectangular glass slides for optical microscopy were first cleaned by sonication in acetone, and then coated by with a 100 nm thick Au film using a commercial sputtering apparatus for metallization of glass surface. This procedure has been shown to make the glass surface less adhesive towards spheres than towards the cantilever surface. A drop of ~ 10 μl of the solution containing the microspheres was spotted onto the Au coated glass slide, and let completely dry for a few minutes. This procedure typically leads to well dispersed microspheres onto the glass slide. Using the XYZ microtranslation stage of the AFM the free end of the cantilever was brought in contact with a single sphere, which was immediately captured by the capillary adhesion force connected to the formation of a water meniscus between the cantilever and the sphere. Upon withdrawal of the cantilever, the sphere gets detached from the substrate that has a lower adhesion, and the chip was then transferred into the oven and was kept for 2 hours at 780^{o}C. After cooling of the system to room-temperature, the colloidal probe was transferred back to the AFM for characterization[60].

Characterization of the probe size and the geometry was done by reverse imaging of the probe on a MikroMasch TGT01 spiked grating. When the probe size is much larger than the features to be imaged, tip-sample convolution is pushed to its limit, resulting in the probe being imaged, instead of the surface features. All measurements were performed in air (RH ~ 40%). Scan areas for probe characterization by reverse imaging were typically 15x15 μm^2, with scan rates of 1-2 Hz and a sampling resolution of about 10 nm/pixel. Three such images were collected and the nominal radius of colloidal probe estimated after analysis was 4624 ± 80 nm.

3.1.2 Point of Zero Charge (PZC) Measurements

PZC estimation of ns-TiOx requires was done using borosilicate colloidal probes. There were four sets of experiment, one with crystalline TiOx and another three with ns-TiOx of varying roughness. Borosilcate coverlip and crystalline TiOx were cleaned in acetone by sonication for 15 mins followed by another round of sonication in Milli-Q water for another 15 mins.

Low concentration buffers were prepared from sodium and potassium salts (1 mM) and pH was stabilized using hydrogen phosphates (0.5 mM). These buffers are low-concentration versions of the standard PBS (Phosphate Buffered Saline) buffer, widely used in biomedical experiments. Buffer solution where made at four different pH values (3, 5, 7 & 9). In literature, pH values for crystalline titanium oxide lies between 3 & 9 which depends on the technique used of measurement and the application of titanium oxide surface [55, 61-62]. Therefore on each surface there were four sets of measurements. At each pH value (3, 5, 7 & 9) 50 FD curves were collected randomly to

accommodate surface disparities due to roughness or any surface adsorbed contaminants. Force curves were collected at scan rate of 0.5 KHz, each made of 512 points. After measurement at one pH, sample and colloidal probe is thoroughly washed with Milli-Q water followed by measurements with same buffer at another pH value.

3.1.3 Buffer Preparation

In order to avoid passivation of surface with ions, very low concentration buffers were used for these experiments. Ion-passivated surfaces would not give us correct value for PZC because screening would smear off any attractive or repulsive forces between AFM probe and titanium oxide surface. The composition of the stock solution which was diluted 100 times with Milli-Q water before each experiment is reported below:

- Potassium Chloride (KCl) – 100 mM
- Sodium Chloride (NaCl) – 100 mM
- Dihydrogen Potassium Phosphate – 50 mM
- Disodium Hydrogen Phosphate - 50 mM

pH of the buffer was adjusted adding Sodium Hydroxide (NaOH) and Hydrogen Chloride (HCl) in mM amounts. Main role of phosphates in any buffer is to stabilize pH of the buffering medium. Very low concentration of phosphates were used in these experiments.

3.1.4 Preparation of Thin Films for AFM Analysis

Uniform ns-TiOx thin films were prepared by SCBD. Thin films prepared were of three different roughness. Film roughness is a monotonically increasing function of film thickness, provided the deposition rate is constant. Roughness and specific area of each surface can be seen in Table-2.

Quantitative characterization of surface morphology of ns-TiO*x* films were done on Nanoscope IV multimode atomic force microscope (Veeco Instruments). The AFM was equipped with rigid cantilevers (resonance frequency 250-300 kHz) with single-crystal silicon tips (nominal radius 5-10 nm), and was operated in Tapping Mode. Typically, several (2-3) 2 μm × 1 μm images (2048 × 1024 points) were acquired on each sample, and flattened by line-by-line subtraction of first and second-order polynomials in order to get rid of the tilt of the sample and of the scanner bow. From flattened AFM images, the average microscale root-mean-square roughness and specific area parameters were calculated.

3.2 Results

3.2.1 Comparison of Surface Chemistry of Crystalline & Ns-TiO_2

To confirm that ns-TiOx and crystalline TiOx have similar surface chemistry we have performed force-volume measurements on nanopatterns of ns-TiOx deposited on crystalline TiOx surfaces produced by NSL/SCBD technique described before. With FV imaging one can clearly identify differential surface chemistry (Figure – 7), because this would likely result in different surface adhesion.

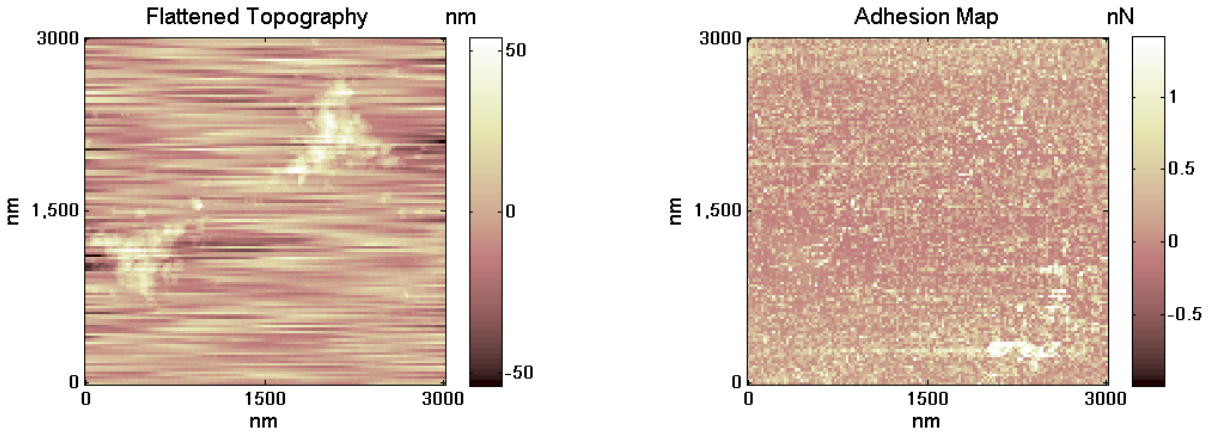

Figure 15. Topography and adhesion map of ns-TiOx patterns produced on crystalline TiOx surface.

Results of FV imaging on crystalline & ns-TiOx demonstrated that both the surface have similar surface chemistry but different surface morphology. Average force of adhesion measured using Silicon Nitride tip against ns-TiOx and Crystalline TiOx is similar, within the experimental error (0.23 ± 0.18 nN and 0.35 ± 0.16 nN, respectively, the smaller adhesion measured on ns-TiOx being related to the rough morphology). In figure 15 differences in topography can be really appreciated whereas on the adhesion map no such difference can be observed. Mechanism of adhesion of Silicon Nitride tip on titanium oxide surface is shown in figure 14. Being the surface chemistry of

crystalline smooth TiOx and nanostructured rough TiOx the same, differences in the PZC can be attributed solely (or primarily) to surface morphology.

3.2.2 Characterization of Surface Morphology of TiOx Samples

PZC measurements were done on four different substrates, crystalline titanium oxide and ns-TiOx of three different roughness. Figures 16 & 17 are TM images of crystalline and ns-titanium oxide along with average roughness (σ). Crystalline TiOx was extremely flat with roughness of 0.1-0.2 nm. It was used as a control to understand the contribution of surface roughness of ns-TiOx towards PZC. Table -2 shows roughness and specific area of each surface used in PZC measurements. Ns-TiOx of three different roughness and specific area (Table -2) were taken for PZC measurements. Data collected from colloidal probe measurements was analyzed using Matlab written routines. All 50 FD curves collected on each sample at each pH were averaged, piezo-displacement coordinates were converted into tip-sample distance coordinates, according to the procedure described in Ref. [7] (i.e. by adding the cantilever deflection to the piezo-displacement axis). Both approaching and retracting curves were collected but only approaching curves were analysed to estimate force experienced by colloidal probe. Reported PZC of Borosilicate glass is between pH 2-3 and our goal was to determine PZC of ns-TiOx [63-64].

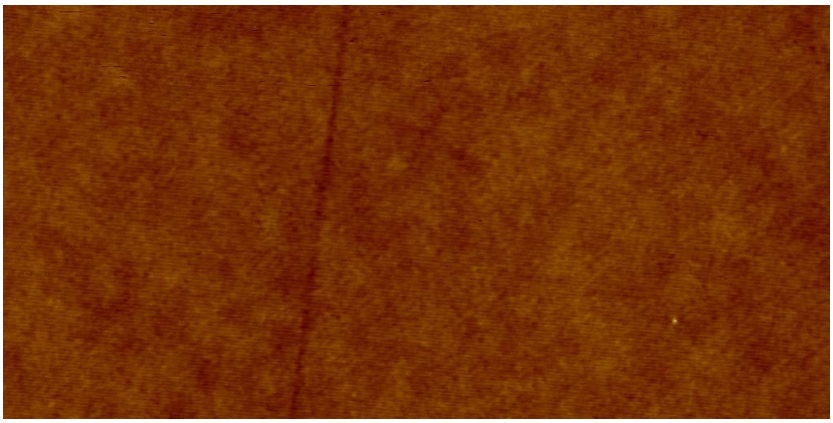

2 x1 µm^2 ; Z Scale– 5 nm

Figure 16. TM Image of crystalline TiOx. (Roughness – 0.13nm ± 0.01 nm)

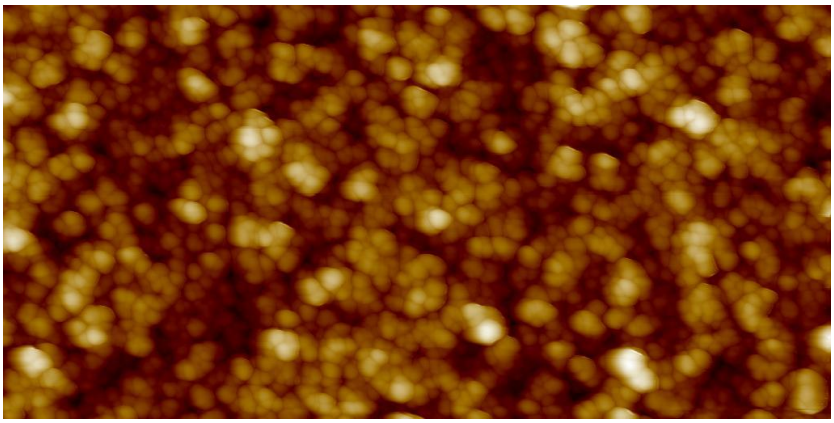

2 x1 µm^2 ; Z Scale – 150 nm

Figure 17. TM Image of ns- TiOx.
(Roughness – 18.5 nm ± 0.69 nm; Specific Area – 1.67 ± 0.08)

Sample	Roughness (σ) (nm)	Specific Area
Crystalline TiOx	0.13 ± 0.01	1.01 ± 0.01
Ns-TiOx (Sample –I)	18.5 ± 0.69	1.67 ± 0.08
Ns-TiOx (Sample –II)	23.95 ± 0.66	1.69 ± 0.02
Ns-TiOx (Sample –III)	26.8 ± 1.77	1.78 ± 0.07

Table 2. Average roughness and specific area of TiOx samples used in PZC experiments.

3.2.3 PZC measurements

Electrostatic forces between the two surfaces are proportional to surface charge densities of the two surfaces. A suitable approximation of Eq. 2, valid for $D>\lambda_D$, is:

$$F_{el} = \frac{4\pi R \lambda_D \sigma_1 \sigma_2}{\varepsilon \varepsilon_o} \times e^{-D/\lambda_D} \qquad (12)$$

Fitting of experimental force vs. distance curves provide values of the prefactor of the exponential, proportional to the product of the two surface charge densities, and of the Debye length, which depends upon the ionic strength of the buffering medium. By plotting $\sigma_1\sigma_2$ (in arbitrary units) as a function of the pH, one can extrapolate at which pH value this product is zero. Under the hypothesis that the PZC of the probe (borosilicate glass) is smaller than 3 (this is confirmed by measurements done with the symmetric system, i.e. borosilicate glass probe vs. borosilicate glass coverslip), the zeroing of $\sigma_1\sigma_2$ identifies the PZC of TiOx. This is explained schematically in Figure 18.

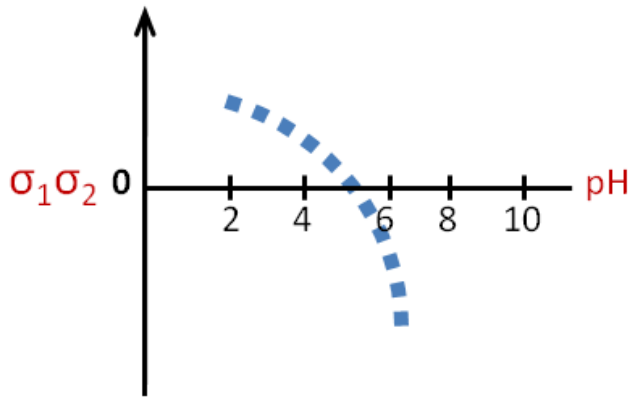

Figure 18. When surface charge density of one of the two surfaces becomes zero that pH value is the point of zero charge of the surface of interest.

Average force curves collected on different sample (the reference crystalline TiO_2 surface and the three rough ns-TiOx surfaces) at different pH values are shown in Figures 19-22. As a general trend, one can notice that the force is repulsive at high pH, become weaker as the pH decreases, and tending to become negligible, in some cases attractive (negative), below pH = 5. In the case of crystalline reference TiO_2, it is clear that the crossing pH value is between pH = 5 and pH = 3, because the sign of the force is reversed. This means that one surface (TiO_2), becomes positively charged, thus resulting in a net attraction between the probe, which is still negatively charged (PZC of the probe is below pH 3). Reporting the actual values of the exponential prefactor proportional to $\sigma_1\sigma_2$ as a function of the pH and carrying out the extrapolation, one obtains that the PZC of rutile TiO_2 is 4.9 ± 0.5 units of pH, a value which is quite consistent with those reported into the literature.

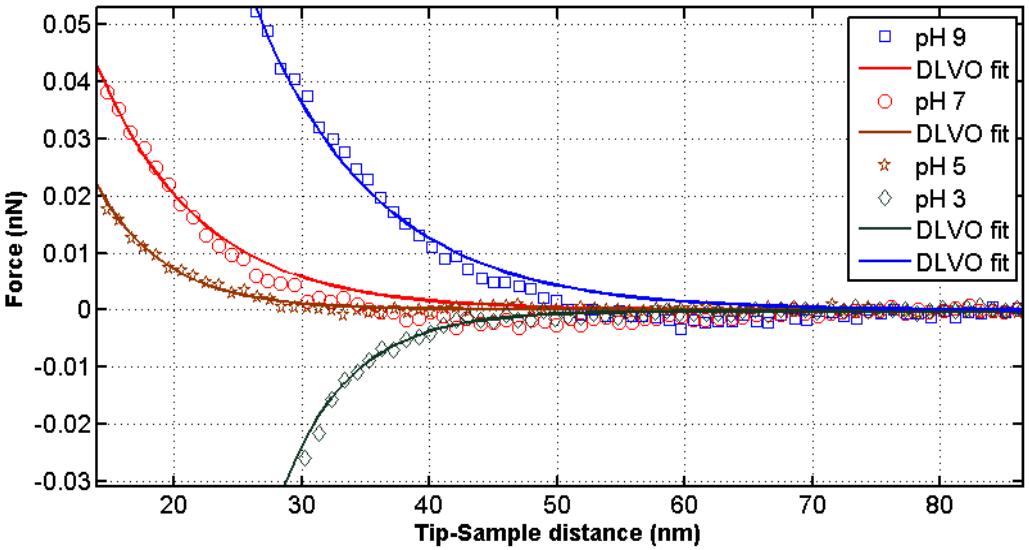

Figure 19. DLVO fitting of force curves on crystalline TiOx surface.

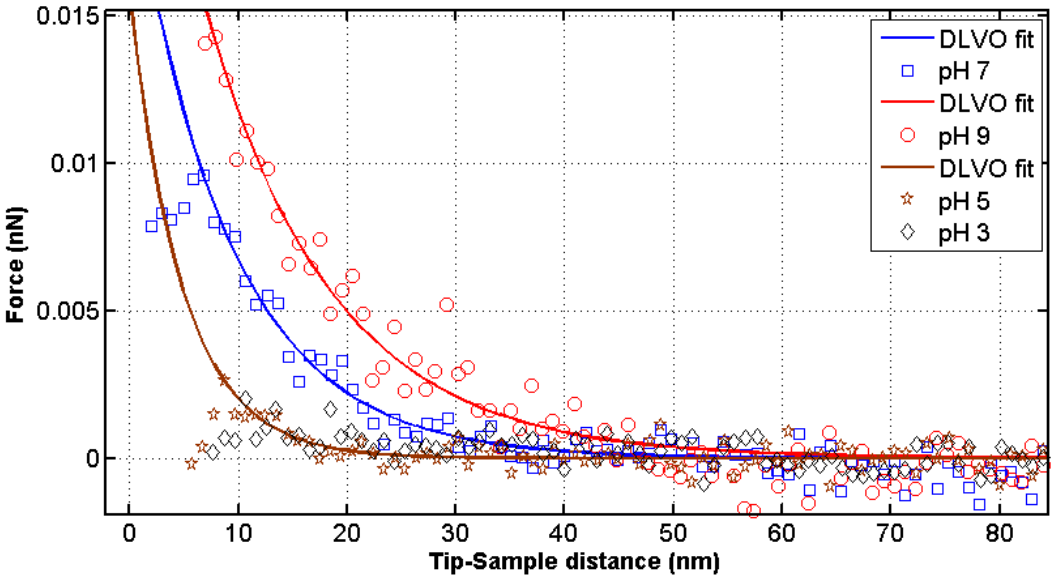

Figure 20. DLVO fitting of force curves on ns-TiOx surface (σ = 18.5 nm ± 0.69)

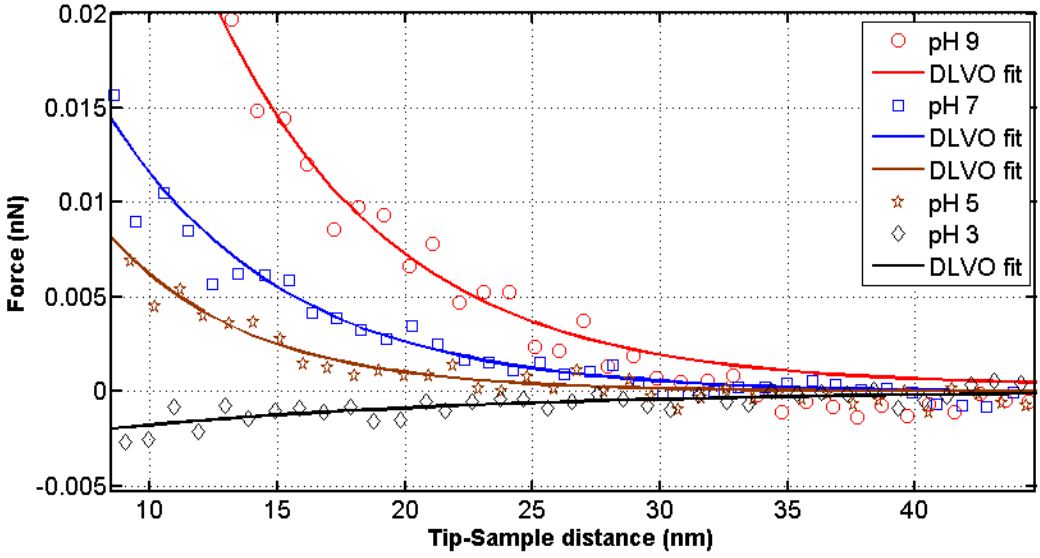

Figure 21. DLVO fitting of force curves on ns-TiOx surface (σ = 23.95 nm ± 0.66)

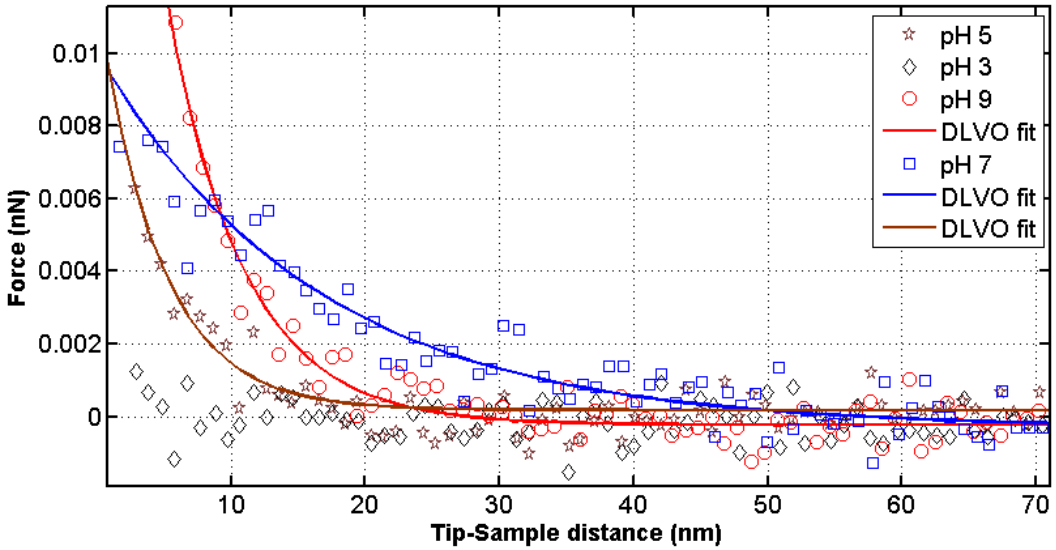

Figure 22. DLVO fitting of force curves on ns-TiOx surface (σ = 26.8 nm ± 1.77).

Repeating the same procedure for the other samples, one obtains the values of PZC for the rough ns-TiOx films. All values are reported in Table 3.

Sample	pH_{PZC}
Borosilicate Glass Probe	< 3
Crystalline TiOx (Rutile)	4.9 ± 0.5
Ns-TiOx (σ = 18.5 nm ± 0.69 nm)	2.5 ± 0.5
Ns-TiOx (σ = 23.95 nm ± 0.66 nm)	3.0 ± 0.5
Ns-TiOx (σ = 26.8 nm ± 1.77 nm)	3.0 ± 0.5

Table 3. Experimentally measured PZC value of different surface.

Figure 23 shows the average force-distance curves collected on all samples at pH = 3. It can be clearly seen that the force of all nanostructured samples is nearly zero, confirming that pH 3 is very close to the actual PZC of nanostructured TiOx films. The force for the crystalline TiO_2 substrate instead is negative, indicating that this specimen has already moved below its PZC, and carries a positive net surface charge, determining an overall attraction to the negtively charged probe.

Figures 23-26 shows a comparison of force-distance curves at each pH, and aim at highlighting the influence of surface roughness on the charging behaviour of ns-TiOx films.

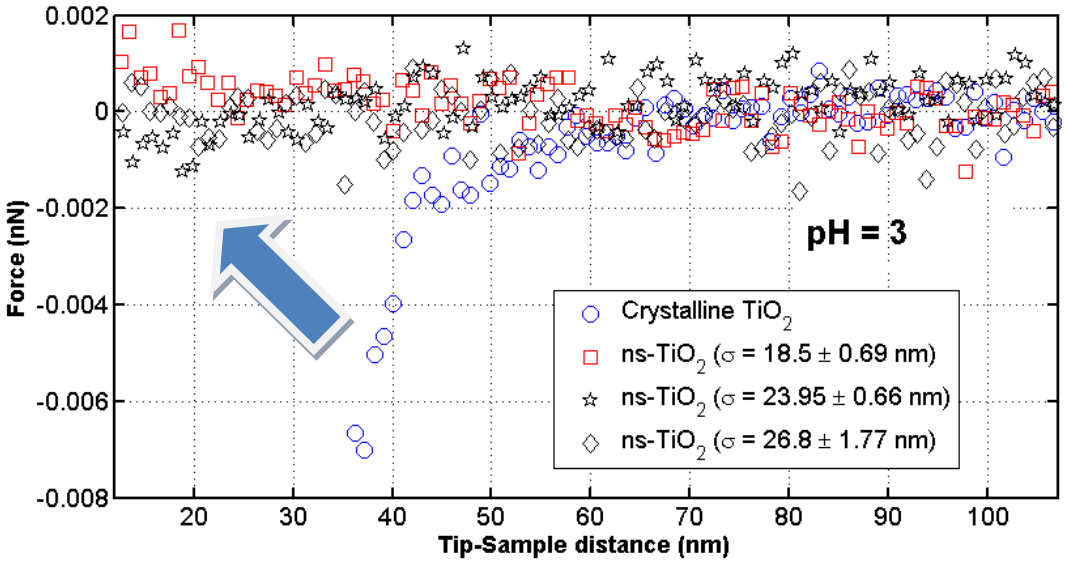

Figure 23. FD curves on crystalline and ns-TiOx at pH 3

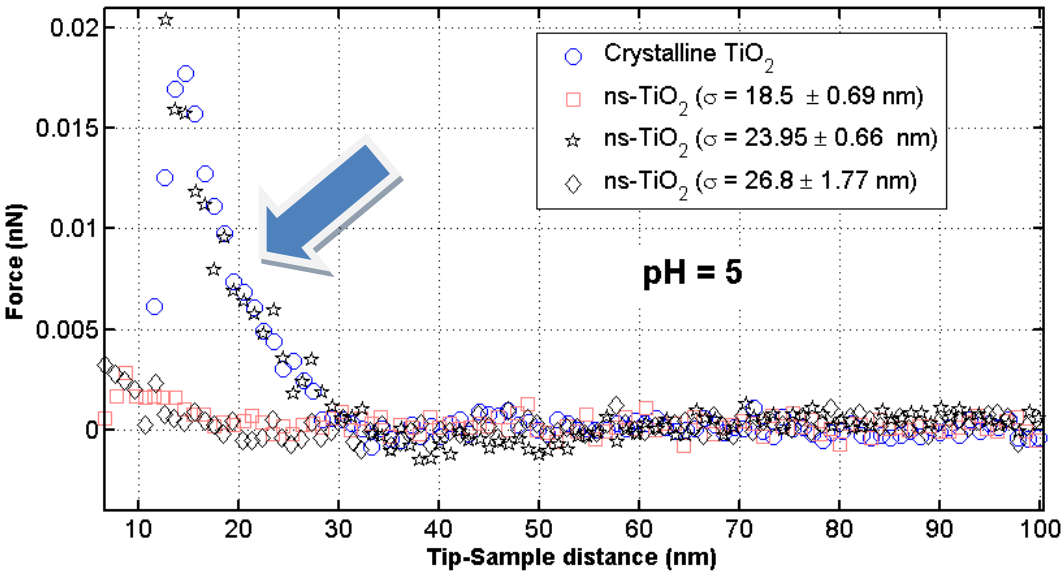

Figure 24. FD curves on crystalline and ns-TiOx at pH 5.

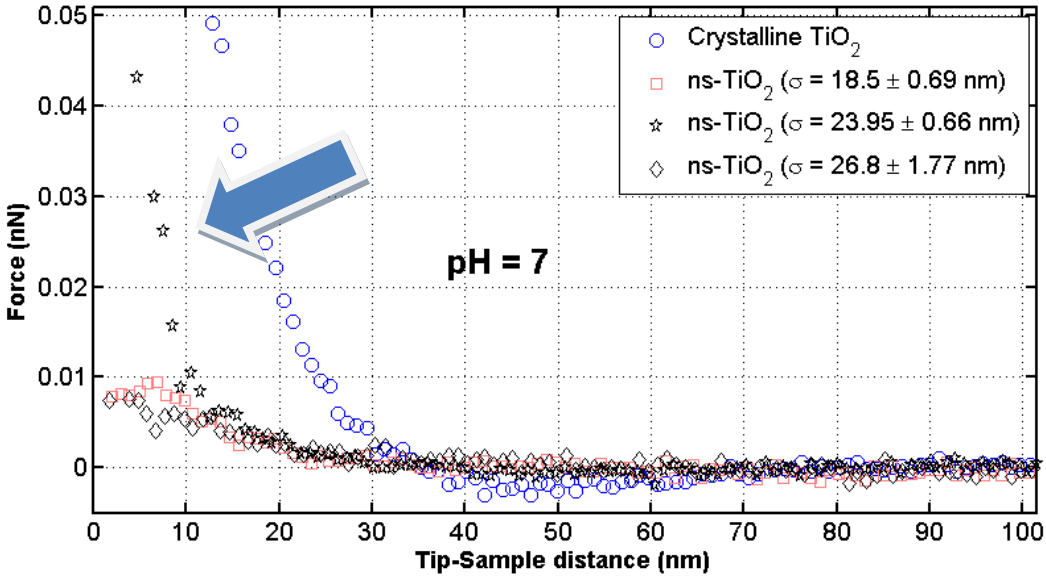

Figure 25. FD curves on crystalline and ns-TiOx at pH 7.

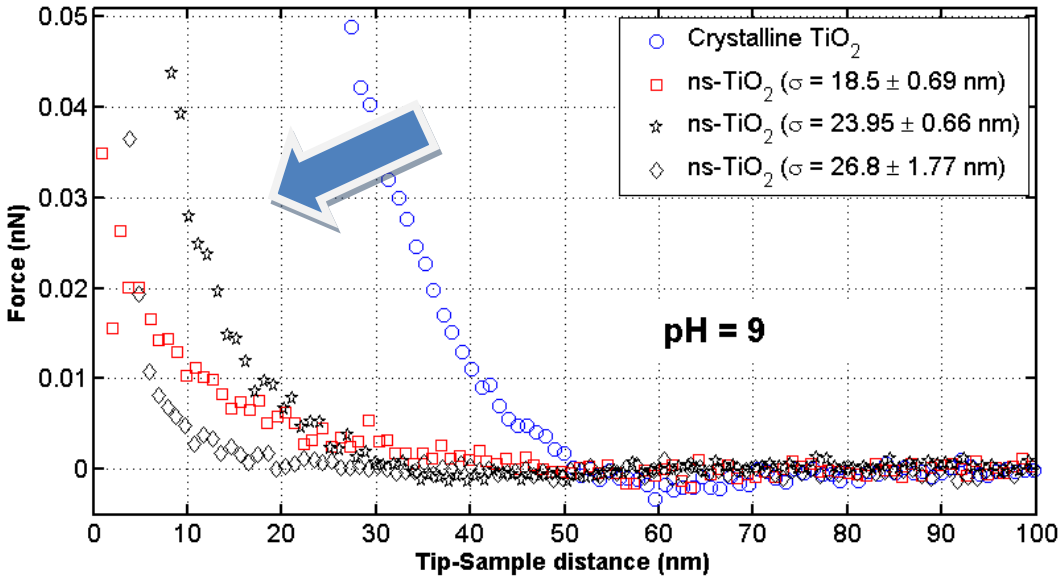

Figure 26. FD curves on crystalline and ns-TiOx at pH 9.

3.3 Discussion

When both the interacting surfaces are at pH above their PZC they will have net negative charge on their surface. As we move from high pH to low pH and when we approach or cross PZC of one of the interacting surface, one can observe reversal of electrostatic forces. In our case PZC of borosilcate glass probe is < 3. Our pH range of investigation is between 3 & 9. Therefore, AFM probe will tend to remain negatively charged at all pH values, and reversal of interaction can be attributed solely to reversal of charging of the TiOx surface, i.e. to crossing of the PZC value of TiOx surfaces.

In case of crystalline TiOx surface this reversal of electrostatic forces can be observed between 5 pH and 3 pH (Figure- 19). PZC of crystalline TiOx surface was estimated to be 4.9 ± 0.5 pH whereas in case of nanostructured Titanium oxides surface it much lower i.e. between pH 2.5-3.0 (Table – 3).

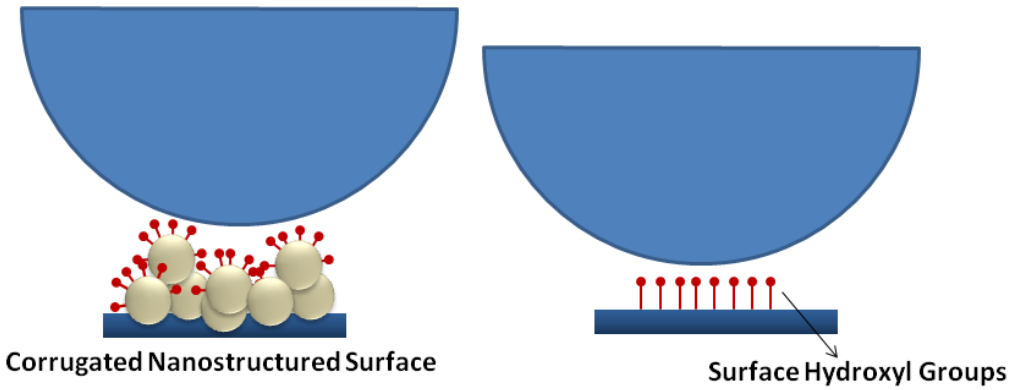

Figure 27. Differential surface hydroxyl distribution on flat crystalline surface (right) and corrugated nanostructured surface (left).

This lower PZC value on nanostructured surface could be due to the effect of surface corrugation (figure-27). In fact, being the surface chemistry of crystalline and nanostructured TiOx very similar (we have proved this by measuring surface adhesion towards the same probe, see section 3.2.1), this conclusion is reasonable and supported by experimental evidence.

A possible interpretation of our findings is the following. Due to surface corrugation (higher specific area) the surface density of hydroxyl groups on ns-TiOx surface is higher compared to flat crystalline surface (see Figure 27). More H^+ ions are required to change net surface charge density from negative to positive. More H^+ ions are available at lower pH, and this shifts the PZC value from 5 towards 3. This is a general influence of the rough morphology. Following this idea, one may expect to find an increasing (repulsive) force, at pH values larger than 3, when the roughness of ns-TiOx films increases. This should be the consequence of increasing the surface charge density in Eq. 11. In fact, although a clear trend is not recognizable in Figures 24-26, some evidence of an opposite trend is observed, i.e. it seems that an increase of surface roughness determines a decrease of the repulsive force. An explanation for this apparent contradiction is that in the presence of surface roughness, the *effective* tip-surface distance is actually larger than that determined from force-distance curves, which reflects the contact the probe establishes with the uppermost protruding asperities. The true distance is approximately $D' = D + D_0$, where D_0 is comparable to the roughness of the film. This shift in the distance axis generates an exponential damping of the overall force (Eq. 11), which can overbalance the increase in the force due to the increase in surface charge due to the gain in specific area.

Bio-chemical properties of titanium oxide surface are greatly influenced by buffering medium. Adsorption characteristics of any biomolecule on a metal oxide surface is affected by following factors:

1. Interaction of buffer with the biomaterial surface
2. Interaction of protein with buffering medium (i.e. role of pH and dissolved ionic species)
3. Direct interaction between bioactive surface and protein molecule.

The study of adhesive properties of ns-TiOx surfaces in milli-q water indicates that in absence of any dissolved ionic species, transition elements like titanium may directly adsorb (chemisorption) protein molecules through coordinate and hydrogen bonding. This will only hold true for those buffers which do not react with metal oxide surface. Many buffers like Tris, HEPES, etc. contain organic molecules, which can bind onto titanium oxide surface in the same manner as any protein molecule, competing with them for adhesion. The binding affinity of these molecules depends in general on pH of the medium. At low concentration, there might be less probability towards direct interaction of protein with metal oxide surface, but at high protein concentration certainly many protein molecules will direct adhere onto titanium oxide surface.

Isoelectric point (IEP) or PZC of a surface is another important parameter which influences proteins adsorption. If net charge on both the surface and a biomolecule is the same, then there won't be any adsorption, because an over all repulsion will be present. That is why it became very important for us to find out PZC of cluster-assembled nanostructured TiOx. In molecular biology almost all proteins are very well

characterized and their IEP values can be easily obtained through literature survey. So, our main objective was to identify PZC of ns-TiOx thin films.

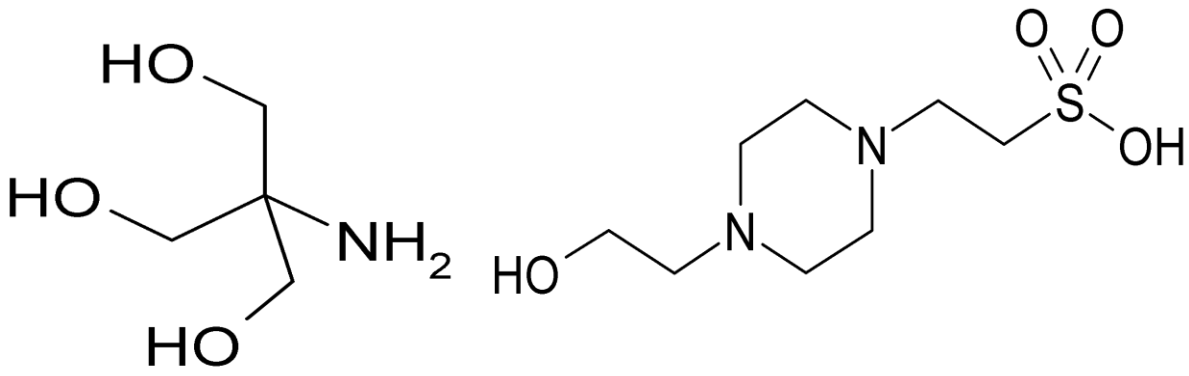

Figure 28. Organic buffers like Tris (left) & HEPES (right) can form coordinative bond with titanium oxide surface in the same manner as any protein molecule

PBS (Phosphate Buffered Saline) is one of the most widely used buffers in molecular biology and is also the favoured buffer for protein adsorption assay. Thus, in order to estimate PZC of TiOx, we created a PBS-like buffer of our own composition, containing very low concentration of salts and concentration of phosphates was kept as low as possible. Concentration of dissolved salts was kept 1 mM and of phosphates 0.5 mM. Phosphates help in stabilizing pH and under ideal circumstances they should not interfere in interactions between substrate and protein molecules, but in case of metal oxide they can interact with metal ions on the surface. In aqueous medium phosphates tend to adhere very strongly to titanium oxide surface [65-66].

Buffers like PBS (Phosphate Buffered Saline) or HBSS (Hank's Buffered Salt Solution) contain high amount of phosphate which may affect adsorption of any protein molecule on its surface. At neutral pH there is a mixture of $\boldsymbol{HPO_4^{2-}}$& $\boldsymbol{H_2PO_4^-}$. With

change in pH, protonation of phosphate groups may affect binding of protein on to the surface. These di-hydrogen and mono-hydrogen phosphates get easily adsorbed onto titanium oxide surface. Along with phosphates other ions like of chloride (Cl^-) can also bind to undercordinated titanium atoms on the surface. They can compete with adsorbed hydroxyl groups and buffers containing high concentration of phosphates can reduce number of hydroxyl groups on the surface.

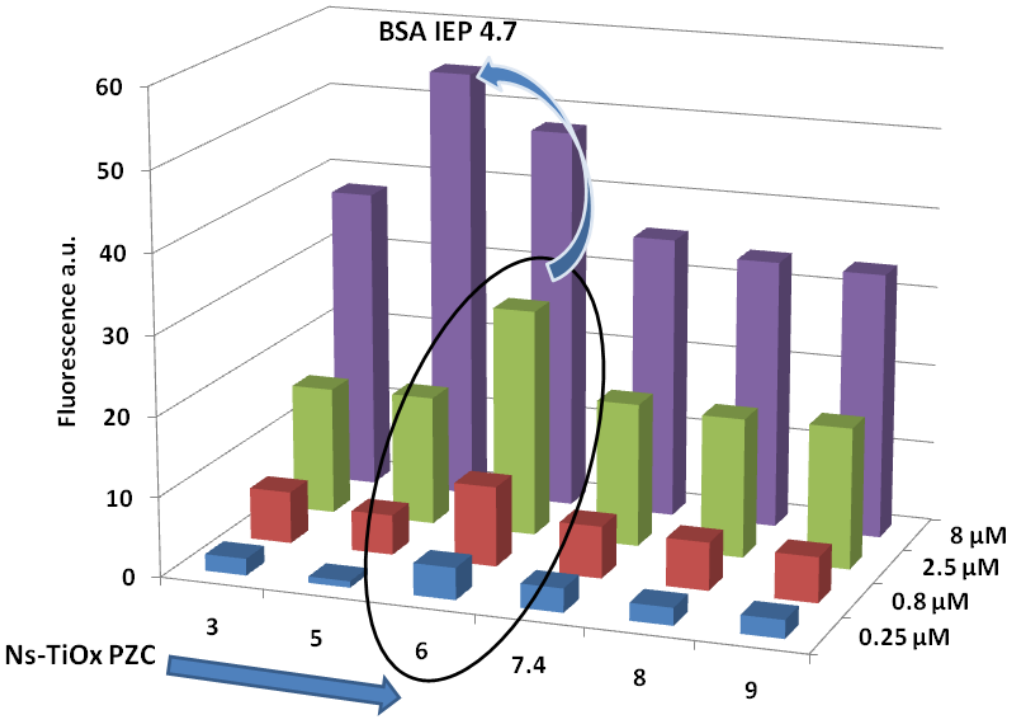

Figure 29. PZC of ns-TiOx shifts from 3 to 6 and maximum protein adsorption takes place from 0.25 µM till 2.5 µM. Then adsorption maxima shifts from 6 to 5 near IEP of BSA. Maximum protein adsorption can take place at the PZC of nanostrucured surface and IEP of BSA.

With the reduction of hydroxyl groups on the surface there can be shifting of PZC of the surface towards higher values and this can affect protein adsorption. This effect can be understood by looking into the data collected by Pasquale Scopelliti from our group [47]. In the figure 29 adsorption profiles of globular protein BSA at different concentrations and at different pH are shown. As we move from low concentration of 0.25 µm to 2.5 µm concentration, we observed adsorption maximum of BSA at pH 6. Then adsorption maxima shifts from pH 6 to pH 5.

Our experimentally determined value of PZC of ns-TiOx is around 3 and IEP of BSA is around 4.7. Hence, adsorption maxima should be expected around 3 or 5, but this is not we have observed. The only possible explanation of this behaviour could be that all BSA adsorption experiments have been done in standard PBS buffer, where concentration of phosphates is very high. These phosphates can easily replace hydroxyl ions on titanium oxide surface, therefore modifying the PZC of the surface. Due to presence of lesser number of hydroxyl groups PZC of the surface can be achieved at higher pH values, because less H^+ ions are required to neutralize the negative charge of ionized hydroxyls; this may shift PZC of the surface from 3 to 6. At pH 6 BSA would have net negative charge on its surface and ns-TiOx surface being electrically neutral it would be much easier for proteins to adsorb on to TiOx on the surface because BSA would experience least repulsion during adsorption. Whereas as we move from 2.5 to 8 µm concentration there is once again shift in adsorption maxima. One possible explanation of this shift could be monolayer formation of BSA on TiOx surface. Once monolayer formation has taken place, then net adsorption of any more protein would depend on net surface charge between protein-protein surface rather than protein-TiOx surface. As

the IEP of BSA is around 4.7-5, adsorbed protein and incoming protein molecules would experience least repulsion. This would allow more adsorption to take place and layering of proteins molecules over each other can take place. This would ultimately shift adsorption maxima to 5. Therefore, one can expect to have adsorption maxima around IEP of proteins or at PZC of nanostructured titanium oxide surface.

Chapter 4 - Conclusion

The objective of this project was to understand interfacial properties of ns-TiOx, and their reliance to interaction of ns-TiOx with proteins and biomolecules. As this nanostructured surface has demonstrated very interesting bioactive properties it became very important to elucidate protein surface interactions.

In particular, the study of adhesive properties of ns-TiOx surfaces in de-ionized milli-q water indicated that in absence of any dissolved ionic species, transition elements like titanium may directly adsorb (chemisorption) protein molecules through coordinate and hydrogen bonding. Moreover, we have characterized the PZC of ns-TiOx in comparison to crystalline TiO2, and found a significant reduction of PZC (from 5 to 3), which cannot entirely be attributed to change insurface chemistry, but is intrinsically related to nanoscale morphology (roughness and specific area).

After the close evaluation of properties of this surface it will be very interesting to better highlight the role of buffering medium in adsorption of protein molecules on its surface. In order to proceed further in understanding interfacial properties ns-TiOx, one should investigate role of different buffers and its interaction with protein and adsorbing surface. By highlighting role of buffering medium, we would like to emphasize that protein adsorption behaviour can be manipulated by using different types of buffering medium. To successfully adapt microarray technology for enzymatic proteins, it is very important to remove any conflicting parameters which may affect their catalytic activity. Adsorption of highly charged species, like phosphates, may affect catalytic properties of any enzyme. As our work has demonstrated that there is high degree of variability in

accumulation of ions on titanium oxide surface, we should take this factor into account when commenting on biochemical activity of adsorbed biomolecules. If we are working other metal oxide surface like zirconium, iron, etc. it will be good if we take in account above described factors into consideration to increase efficacy of protein adsorption and at the same time retain complete bioactivity of adsorbed protein molecule.

Appendix

AFM Tip Functionalization with –COOH Groups

AFM tips were functionationalized using PEG (polyethylene glycol) linker. First PEG linker is modified to produce Di-Imidazolyl-Terminated PEG (PEG-Im2). Henceforth, this modified linker is used in tip functionalization [67].

XPS Analysis - High-resolution C 1s scans provided more precise information about PEG –COOH linker. The contributions of CO, OCN and COOH are indicated in the figure 30. This data indicates presence of PEG linker attached to the silicon substrate and the free end of the linker is functionalized with –COOH group.

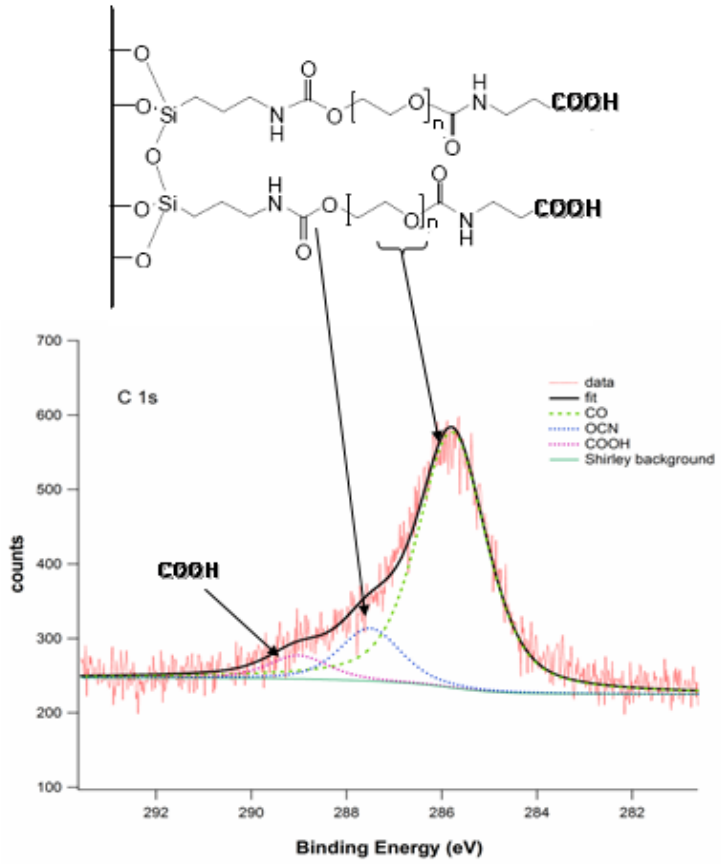

Figure 30. XPS Analysis of Fuctionalized Surface
Courtesy - Dr. C. Lenardi

AFM-Force Spectroscopy **-** Force spectroscopy experiment was conducted on regular non-patterned ns-TiOx thin films in PBS buffer. Forces vs. distance (FD) curves of functionalized tips were carried at low scan rate of 0.5 hz. Preliminary measurements for functionalized tips were carried out. A number of FD curves were obtained against ns-TiOx thin film to verify functionalization and binding of carboxylic groups to ns-TiOx surface. Result is indicated in Figure 31. Extension of the linker takes place after carboxylic group forms a bond with ns-TiOx surface.

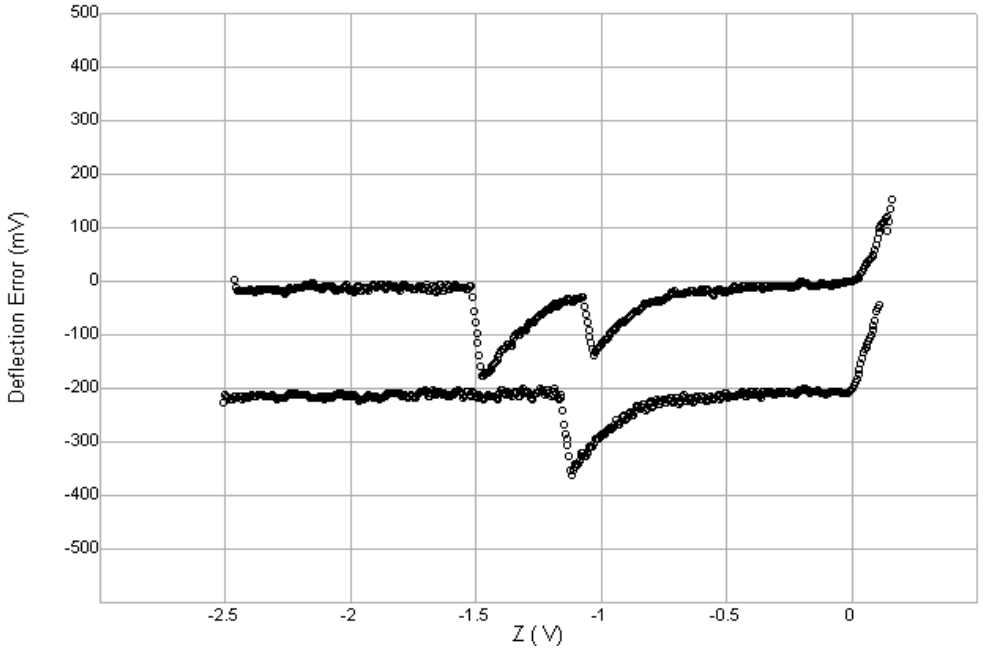

Figure 31. A typical force vs. distance curve. COOH group bind to ns-TiOx surface and extension of the PEG linker can be observed.

These are only the initial results of the experiments and only raw data is presented here. More extensive data analysis is required for quantifying binding strength of carboxylic group with titanium atoms on nanostructured surface.

Mobility of Metal Oxide Nanoclusters Over Silicon Oxide Surface.

Sample for both ns-TiOx and ns-PdOx were prepared by coupling SCBD with NSL. After removal of the spheres both ns-TiOx and ns-PdOx samples were annealed at 300^{O}C, 450^{O}C and 600^{O}C. After each step of annealing both samples were imaged in tapping mode with AFM to understanding and observe any mobility of clusters with increasing temperature. Thereafter, Images of patterned substrates were taken in tapping mode, at scan rate of 1-2 Hz. Scan size of images was 5 and 20 µm for visualization of any changes in nanoscale patterns.

Results & Discussion - Both the samples of patterned ns-TiOx and ns-PdOx were gradually annealed at 300 ^{o}C, 450 ^{o}C and 600 ^{o}C. After imaging them with AFM one can comment on behaviour of nano-clusters on amorphous silica substrate. In figure 32 one can observe changes with ns-PdOx. As we anneal as-deposited (as-dep in figure 32) to 300 ^{o}C there is an increase in number of small nano-particle/clusters of ns-PdOx on glass substrate, plus they start to grow to larger size over thin-filmed triangular islands. On increasing the temperature to 450 ^{o}C crystallite formation takes place. Size of the crystals is much larger over triangular island films. On further annealing to 600 ^{o}C, there is change in shape of crystals. They become more spherical in shape. This could be due to change of crystalline phase as we anneal the same sample to 600 ^{o}C. By carefully examining the images we may conclude that after pinning of the ns-PdOx clusters on the surface they tend to grow into bigger sized crystallites.

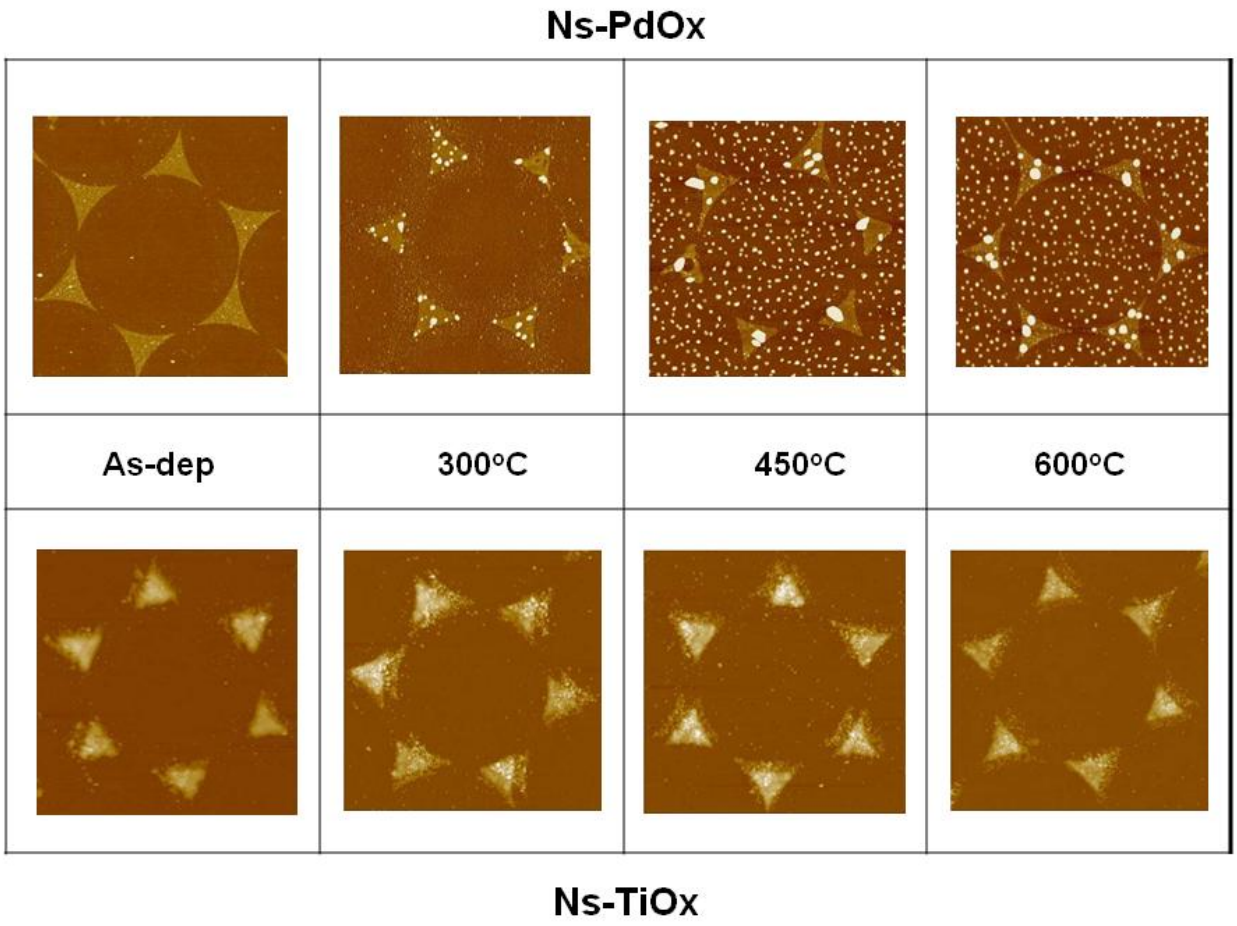

Figure 32. AFM images of patterned ns-TiOx(5 μm^2 & Z scale – 150 nm) and ns-PdOx(5 μm^2 & Z scale – 50 nm). (a)With increasing temperature one can observe gradual changes with ns-PdOx. At 300^oC clusters become mobile they start to grow in size and at 450 ^oC crystallite formation can be observed, whereas 600 ^oC crytalloids tend to become more spherical.(b) There are no observed changes with ns-TiOx. With increasing annealing temperature they retain their as-dep morphology

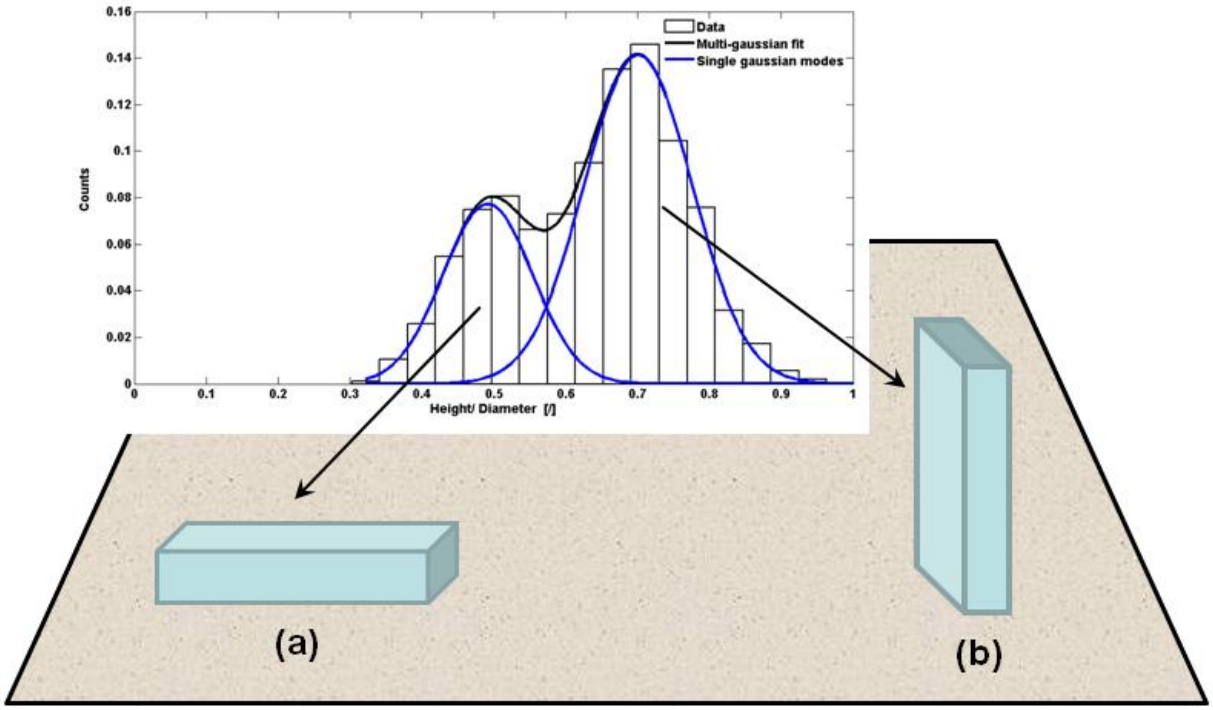

Figure 33. Crystals are growing on the substrate in two different orientations at 450^{o}C. Type (a) grow more horizntally and type (b) grow more vertically. On estimating Height/Diameter ratio of different crsytals one can observe that there are more number of crystals growing in vertical manner

Height to Diameter ratio was also analyzed for sample at 300 ^{o}C and 600 ^{o}C. At 600 ^{o}C peaks shift towards left indicating that crystallites have become more spherical in shape. This can also be observed directly by visual inspection of images. All the crystalline features are evenly distributed over the substrate.More detailed analysis of images at 450 ^{o}C we observed two different populations of crystals growing on the substrate. In figure 33 type (a) crystals grow horizontally on substrate whereas another type (b) grow more vertically. This growth pattern was analyzed by comparing Height to Diameter ratio of each crystalline feature growing on the amorphous silicon oxide.

There were no observed changes in the morphology of ns-TiOx. We could not observe any mobility among TiOx clusters or any changes in TiOx thin films in form of triangular islands. One possible explanation could be chemical bond formation between silicon oxide substrate and titanium oxide clusters. Both titanium and silicon are known to form oxide linkages [68]. During initial annealing at low temperature (300 ^{o}C) loosely attached clusters may form interconnecting oxygen linkages with silicon. This will permanently immobilize them on the surface, therefore we could not observe any cluster mobility in ns-TiOx samples.

TPD Patterning Through NSL

TPD is a biphenyl molecule which is used in producing organic LEDs (OLEDs). This material can be deposited by Physical Vapour Deposition (PVD) or can be easily evaporated onto the target surface. After production of monolayer of polystyrene spheres by NSL, TPD was deposited by PVD. After the removal of spheres, TPD pattern was imaged in tapping mode. Height of each TPD pillar is approximately 1.5 microns. TPD can be deposited over a thin film of Indium Tin Oxide (ITO) which is a transparent conductive layer to form contacts for electrodes [69-70] .

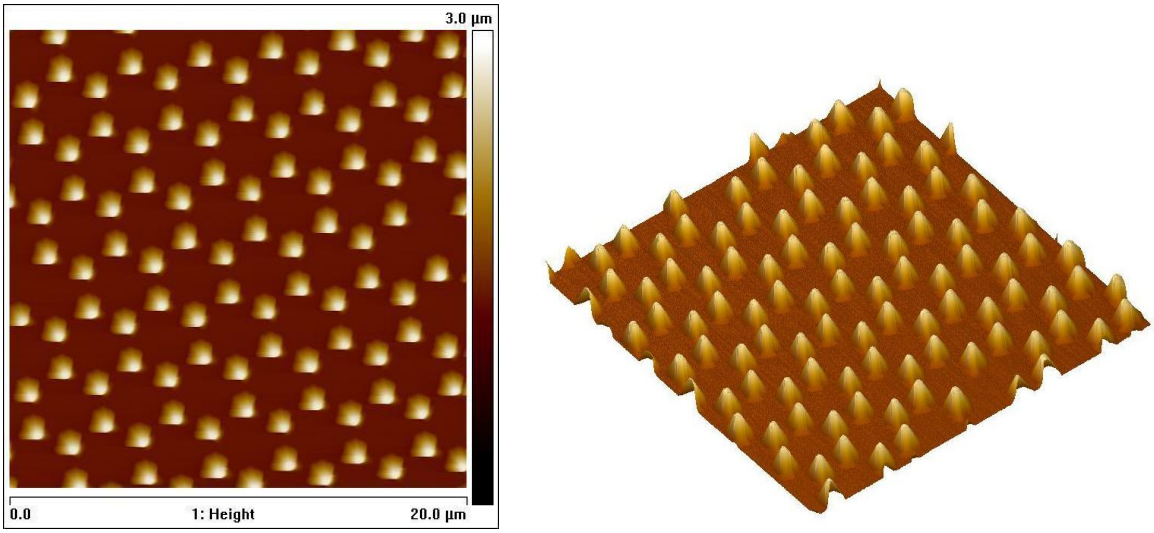

Figure 34. 2D hexagonal array of TPD pillars produced by physical vapor deposition using NSL

Behaviour of PC12 Cells on crystalline and ns-TiOx

PC12 cells were grown on crystalline and patterned ns-TiOx. The main objective of this work was to explore function of cell spreading, cell area and cell morphology in relation to morpho-chemical variations in the substrate. By studying cell spreading function one can observe selective preference of PC12 cells for nanostructured surface as compared to crystalline surface. In the figure 35 one can see how cell membranes in a group of cells are merging together and forming intracellular network. In figure 36 cells were grown over patterned ns-TiOx surface on crystalline TiOx surface. One can see complete spreading of cell over both nanostructured and crystalline TiOx. With larger patterns one would be able to appreciate selective cell spreading on either ns or crystalline TiOx surface [71] .

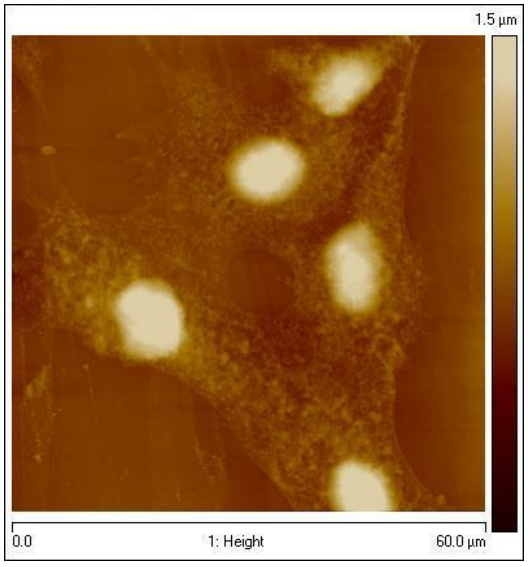

Figure 35. Intracellular network of PC12 cells on crystalline TiOx surface.

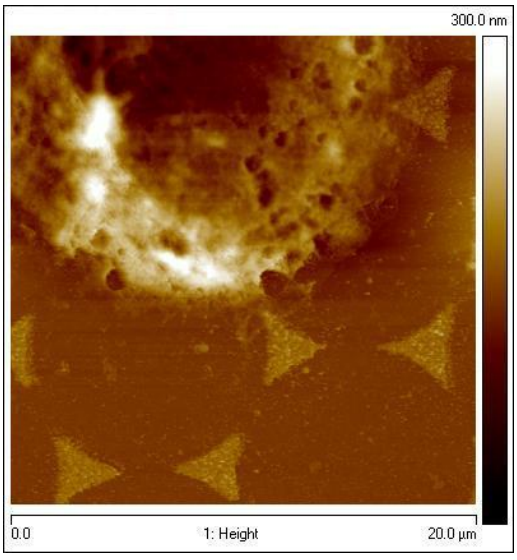

Figure 36. Cell spreading over patterned ns-TiOx and crystalline TiOx.

Bacterial Biofilm Formation Over ns-TiOx.

Ns-TiOx is not only a good substrate to grow various human cell lines but can also be used to study proliferation of clinically relevant bacterial species. In this case we have studied growth of E. Coli on nanostructured surface. Figure 42 is a phase image of bacterial growth over ns-TiOx. As one can see in phase image, contrast between the background surface and bacteria is very good. This may be due to the fact that prokaryote secretes lesser amount of proteins as compared to eukaryotes. Because of this fact there is also a possibility that their peptidoglycan cell wall can directly with titanium oxide surface, which is not the case in eukartyotic systems as cell spreading behaviour is affected layering of protein molecules between substrate and the cell membrane [72].

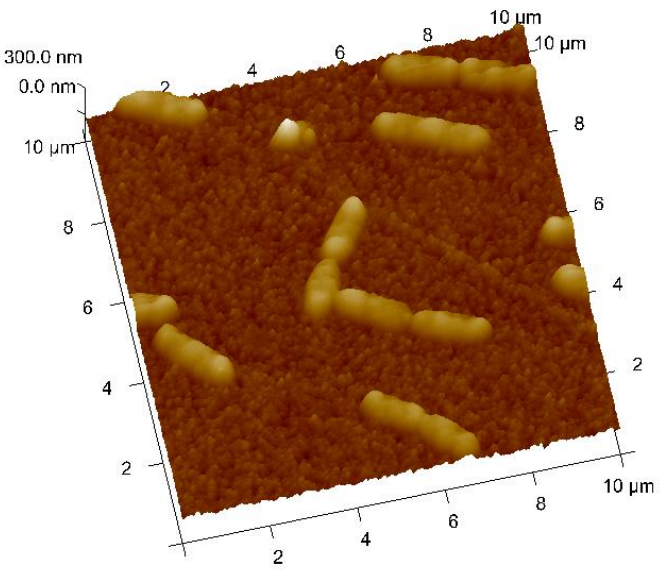

Figure 37. 3D image of EColi over ns-TiOx

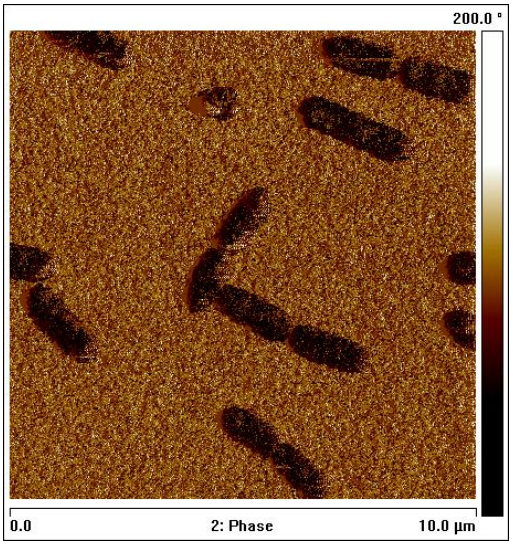

Figure 38. Phase image of E.Coli on ns-TiOx

Bibliography

1. Bhushan, B., *Springer Handbook of Nanotechnology*. 2006: Springer Verlag.
2. Valentine, A.M., *Titanium: Inorganic & Coordination Chemistry*. Encyclopedia of Inorganic Chemistry. 2006: John Wiley & Sons, Ltd.
3. Brunette, D., P. Tengvall, and M. Textor, *Titanium in Medicine: Material Science, Surface Science, Engineering, Biological Responses and Medical Applications (Engineering Materials)*. 2001: Springer.
4. Carbone, R., et al., *Retroviral microarray-based platform on nanostructured TiO2 for functional genomics and drug discovery.* Biomaterials, 2007. **28**(13): p. 2244-2253.
5. Carbone, R., et al., *Biocompatibility of cluster-assembled nanostructured TiO2 with primary and cancer cells.* Biomaterials, 2006. **27**(17): p. 3221-3229.
6. Hinterdorfer, P. and Y.F. Dufrêne, *Detection and localization of single molecular recognition events using atomic force microscopy.* Nature Methods, 2006. **3**(5): p. 347-355.
7. Butt, H.J., B. Cappella, and M. Kappl, *Force measurements with the atomic force microscope: Technique, interpretation and applications.* Surface Science Reports, 2005. **59**(1): p. 1-152.

8. Derjaguin, B.V. and L. Landau, *Theory of stability of highly charged lyophobic sols and adhesion of highly charged particles in solutions of electrolytes.* Acta Physicochim. URSS, 1941. **14**: p. 633–52.

9. Verwey, E.J.W. and J. Overbeek, *Theory of the stability of lyophobic colloids.* Elsevier Publ. Co. Inc., London, 1948. **8**(8): p. 9.

10. Jolivet, J., *Metal Oxide Chemistry & Synthesis: From Solution to Oxide*. 2000: John Wiley & Sons Ltd.

11. Pechenyuk, S., *The use of the pH at the point of zero charge for characterizing the properties of oxide hydroxides.* Russian Chemical Bulletin, 1999. **48**(6): p. 1017-1023.

12. Nelson, D. and M. Cox, *Lehninger Principles of Biochemistry, Fourth Edition*. 2004: W. H. Freeman.

13. Butt, H.J., *Measuring electrostatic, van der Waals, and hydration forces in electrolyte solutions with an atomic force microscope.* Biophysical Journal, 1991. **60**(6): p. 1438-1444.

14. Raiteri, R., B. Margesin, and M. Grattarola, *An atomic force microscope estimation of the point of zero charge of silicon insulators.* Sensors and Actuators B: Chemical, 1998. **46**(2): p. 126-132.

15. Xu, L.-C. and C.A. Siedlecki, *Effects of surface wettability and contact time on protein adhesion to biomaterial surfaces.* Biomaterials, 2007. **28**(22): p. 3273-3283.

16. Philip, M., *Nanostructured materials.* Reports on Progress in Physics, 2001(3): p. 297.

17. Gleiter, H., *Nanostructured materials: basic concepts and microstructure.* Acta Materialia, 2000. **48**(1): p. 1-29.

18. Barborini, E., P. Piseri, and P. Milani, *A pulsed microplasma source of high intensity supersonic carbon cluster beams.* Journal of Physics D: Applied Physics, 1999. **32**(21): p. L105-L109.

19. Wegner, K., et al., *Cluster beam deposition: a tool for nanoscale science and technology.* Journal of Physics D: Applied Physics, 2006. **39**: p. R439.

20. Scopelliti, P.E., et al., *The Effect of Surface Nanometre-Scale Morphology on Protein Adsorption.* PLoS ONE, 2010. **5**(7): p. e11862.

21. Giorgetti, L., et al., *Adsorption and Stability of Streptavidin on Cluster-Assembled Nanostructured TiOx Films.* Langmuir, 2008. **24**(20): p. 11637-11644.

22. Singh, A.V. and et al., *A simple lift-off-based patterning method for micro- and nanostructuring of functional substrates for cell culture.* Journal of Micromechanics and Microengineering, 2009. **19**(11): p. 115028.

23. Indrieri, M., *Quantitative Characterization of Biological Systems at Single Molecule Level by Atomic Force Microscopy*, in *Department of Physics*. 2007, University of Milan: Milan,Italy.

24. Butt, H.-J. and M. Kappl, *Normal capillary forces.* Advances in colloid and interface science, 2009. **146**(1-2): p. 48-60.

25. Junno, T., et al., *Contact mode atomic force microscopy imaging of nanometer-sized particles.* Applied Physics Letters, 1995. **66**(24): p. 3295-3297.

26. Heinz, W.F. and J.H. Hoh, *Spatially resolved force spectroscopy of biological surfaces using the atomic force microscope.* Trends in Biotechnology, 1999. **17**(4): p. 143-150.

27. Willemsen, O.H., et al., *Biomolecular Interactions Measured by Atomic Force Microscopy.* Biophysical Journal, 2000. **79**(6): p. 3267-3281.

28. García, R. and R. Pérez, *Dynamic atomic force microscopy methods.* Surface Science Reports, 2002. **47**(6-8): p. 197-301.

29. Möller, C., et al., *Tapping-Mode Atomic Force Microscopy Produces Faithful High-Resolution Images of Protein Surfaces.* Biophysical Journal, 1999. **77**(2): p. 1150-1158.

30. Cheung, C.L., et al., *Fabrication of nanopillars by nanosphere lithography.* Nanotechnology, 2006. **17**(5): p. 1339-1343.

31. Hulteen, J.C. and R.P. Van Duyne, *Nanosphere lithography: A materials general fabrication process for periodic particle array surfaces.* Journal of Vacuum Science & Technology A: Vacuum, Surfaces, and Films, 1995. **13**(3): p. 1553-1558.

32. Sader, J.E., et al., *Method for the calibration of atomic force microscope cantilevers.* Review of Scientific Instruments, 1995. **66**(7): p. 3789-3798.

33. Barabasi, A.L. and H.E. Stanley, *Fractal Concepts in Surface Growth*. 1995: Cambridge University Press.

34. Podestà, A., et al., *Cluster-Assembled Nanostructured Titanium Oxide Films with Tailored Wettability.* The Journal of Physical Chemistry C, 2009. **113**(42): p. 18264-18269.

35. Wenzel, R.N., *Resistance of Solid Surfaces to Wetting by Water.* Industrial & Engineering Chemistry, 1936. **28**(8): p. 988-994.

36. Takeda, S., et al., *Surface OH group governing adsorption properties of metal oxide films.* Thin Solid Films, 1999. **339**(1-2): p. 220-224.

37. Bergström, L., *Hamaker constants of inorganic materials.* Advances in Colloid and Interface Science, 1997. **70**: p. 125-169.

38. Peressadko, A.G., N. Hosoda, and B.N.J. Persson, *Influence of Surface Roughness on Adhesion between Elastic Bodies.* Physical Review Letters, 2005. **95**(12): p. 124301.

39. Israelachvili, J., *Intermolecular and Surface Forces*. 2nd ed. 1991: Academic Press.

40. Barborini, E., et al., *Supersonic cluster beam deposition of nanostructured titania.* The European Physical Journal D - Atomic, Molecular, Optical and Plasma Physics, 2003. **24**(1): p. 277-282.

41. Bergström, L. and E. Bostedt, *Surface chemistry of silicon nitride powders: Electrokinetic behaviour and ESCA studies.* Colloids and Surfaces, 1990. **49**: p. 183-197.

42. Lin, X.Y., F. Creuzet, and H. Arribart, *Atomic force microscopy for local characterization of surface acid-base properties.* The Journal of Physical Chemistry, 1993. **97**(28): p. 7272-7276.

43. Raiteri, R., S. Martinoia, and M. Grattarola, *pH-dependent charge density at the insulator-electrolyte interface probed by a scanning force microscope.* Biosensors and Bioelectronics, 1996. **11**(10): p. 1009-1017.

44. Bullard, J.W. and M.J. Cima, *Orientation Dependence of the Isoelectric Point of TiO2 (Rutile) Surfaces.* Langmuir, 2006. **22**(24): p. 10264-10271.

45. Senden, T.J. and C.J. Drummond, *Surface chemistry and tip-sample interactions in atomic force microscopy.* Colloids and Surfaces A: Physicochemical and Engineering Aspects, 1995. **94**(1): p. 29-51.

46. Busca, G., et al., *FT-IR characterization of silicon nitride Si3N4 and silicon oxynitride Si2ON2 surfaces.* Journal of Molecular Structure, 1986. **143**: p. 525-528.

47. Zhuravlev, L.T., *The Surface Chemistry of Amorphous Silica. Zhuravlev Model.* Colloids and Surfaces A: Physiochemical and Engineering Aspects 2000. **173**: p. 1-38.

48. Tamura, H., et al., *Surface Hydroxyl Site Densities on Metal Oxides as a Measure for the Ion-Exchange Capacity.* Journal of Colloid and Interface Science, 1999. **209**(1): p. 225-231.

49. Hoh, J. and J. Revel, *Tip-sample interactions in atomic force microscopy: I. Modulating adhesion between silicon nitride and glass.* Nanotechnology, 1991. **2**: p. 119.

50. Caruso, T., et al., *Electronic Structure of Cluster Assembled Nanostructured TiO2 by Resonant Photoemission at the Ti L2,3 Edge.* Jounal of Chemical Physics, 2008. **128**: p. 094704-711

51. Barborini, E., et al., *Nanostructured TiO2 Films with 2 eV Optical Gap.* Advanced Materials, 2005. **17**(15): p. 1842-1846.

52. Caruso, T., et al., *Photoemission investigations on nanostructured TiO2 grown by cluster assembling.* Surface Science, 2007. **601**(13): p. 2688-2691.

53. Brookes, I.M., C.A. Muryn, and G. Thornton, *Imaging Water Dissociation on TiO_{2}(110).* Physical Review Letters, 2001. **87**(26): p. 266103.

54. Schaub, R., et al., *Oxygen Vacancies as Active Sites for Water Dissociation on Rutile TiO_{2}(110).* Physical Review Letters, 2001. **87**(26): p. 266104.

55. Diebold, U., *The surface science of titanium dioxide.* Surface Science Reports, 2003. **48**(5-8): p. 53-229.

56. Conti, M., G. Falini, and B. Samorì, *How Strong Is the Coordination Bond between a Histidine Tag and Ni – Nitrilotriacetate? An Experiment of Mechanochemistry on Single Molecules.* Angewandte Chemie, 2000. **112**(1): p. 221-224.

57. Fukuzaki, S., H. Urano, and K. Nagata, *Adsorption of bovine serum albumin onto metal oxide surfaces.* Journal of Fermentation and Bioengineering, 1996. **81**(2): p. 163-167.

58. Giacomelli, C.E., M.J. Avena, and C.P. De Pauli, *Adsorption of Bovine Serum Albumin onto TiO2Particles.* Journal of Colloid and Interface Science, 1997. **188**(2): p. 387-395.

59. Dean, P.M., *Molecular Foundations of Drug Receptor Interactions*: Cambridge University Press; Cambridge, 1987.

60. Marco Indrieri; Alessandro Podesta'; Gero Bongiorno; Davide Marchesi; Paolo Milani, *Production and characterization of epoxy-free colloidal probes for atomic force microscopy.* Submitted to Ultramicroscopy, 2010.

61. Preocanin, T. and N. Kallay, *Point of Zero Charge and Surface Charge Density of TiO~ 2 in Aqueous Electrolyte Solution as Obtained by Potentiometric Mass Titration.* Croatica chemica acta, 2006. **79**(1): p. 95.

62. Kosmulski, M., *The significance of the difference in the point of zero charge between rutile and anatase.* Advances in Colloid and Interface Science, 2002. **99**(3): p. 255-264.

63. Barz, D.P.J., M.J. Vogel, and P.H. Steen, *Determination of the Zeta Potential of Porous Substrates by Droplet Deflection. I. The Influence of Ionic Strength and pH Value of an Aqueous Electrolyte in Contact with a Borosilicate Surface.* Langmuir, 2009. **25**(3): p. 1842-1850.

64. Harame, D.L., et al., *Ion-sensing devices with silicon nitride and borosilicate glass insulators.* Electron Devices, IEEE Transactions on, 1987. **34**(8): p. 1700-1707.

65. Connor, P.A. and A.J. McQuillan, *Phosphate Adsorption onto TiO2 from Aqueous Solutions: An in Situ Internal Reflection Infrared Spectroscopic Study.* Langmuir, 1999. **15**(8): p. 2916-2921.

66. Michelmore, A., et al., *The interaction of linear polyphosphates with titanium dioxide surfaces.* Physical Chemistry Chemical Physics, 2000. **2**(13): p. 2985-2992.

67. Ranucci, E. and P. Ferruti, *A New Synthetic Method for Amino-Terminated Poly (Ethyleneglycol) Derivatives.* Synthetic Communications: An International Journal for Rapid Communication of Synthetic Organic Chemistry, 1990. **20**(19): p. 2951 - 2957.

68. Fu, X., et al., *Enhanced Photocatalytic Performance of Titania-Based Binary Metal Oxides: TiO2/SiO2 and TiO2/ZrO2.* Environmental Science & Technology, 1996. **30**(2): p. 647-653.

69. Celii, F., T. Harton, and O.F. Phillips, *Characterization of organic thin films for OLEDs using spectroscopic ellipsometry.* Journal of Electronic Materials, 1997. **26**(4): p. 366-371.

70. Viola, I., et al., *Positive/Negative Arrays of Organic Light-Emitting Diodes by a Surface-Tension-Driven Approach.* Advanced Materials, 2005. **17**(24): p. 2935-2939.

71. Singh, A.V., et al., *A simple lift-off-based patterning method for micro- and nanostructuring of functional substrates for cell culture*. 2009, IOP.

72. Gristina, A. and J. Costerton, *Bacterial adherence to biomaterials and tissue. The significance of its role in clinical sepsis.* J Bone Joint Surg Am, 1985. **67**(2): p. 264-273.

Publications

- Probing nanoscale interactions on biocompatible cluster-assembled Titanium Oxide surfaces by Atomic Force Microscopy; ***Varun Vyas,*** *Alessandro Podesta, Paolo Milani*; Journal of Nanoscience and Nanotechnology (2010) (In Press).

Acknowledgements

I would like to acknowledge advice and guidance of my supervisors Prof. Paolo Milani and Dr. Alessandro Podesta'. I would also like to offer my graditude to my colleagues Dr. Marco Indrieri, Simone Bovio, Massimiliano Galluzzi, Ajay Singh and other lab members for being always available for discussions during the course of this project.

I offer special thanks to European School of Molecular Medicine (SEMM) for supporting research grant for Medical Nanotechnology Program.